ilset

July 15-19
Washington, DC
USA
2020

Proceedings of International Conference on

Life Sciences, Engineering and Technology

July 15-19, 2020 Washington, DC, USA

Editors

Dr. Vaughn M. Bradley
Dr. Ismail Sahin

istes Organization

www.ilset.net

Volume 1, Pages 1-36

Proceedings of International Conference on Life Sciences, Engineering and Technology

ISBN: 978-1-952092-09-1

Edited by: Vaughn M. Bradley & Ismail Sahin

Articles: 1-7

Conference: International Conference on Life Sciences, Engineering and Technology (iLSET)

Dates: July 15-19, 2020

Location: Washington, DC, USA

Conference Chair(s):

Richard Thripp, University of Central Florida, USA

Vaughn M. Bradley, Walden University, USA

The submissions are subject to a double-blind peer review process by at least two reviewers with expertise in the relevant subject area. the review policy is available at the conference web page: www.ilset.net

Table of Contents

The Constant K and the Gaussian Temporal Evolution for COVID-19

Antonio J. Balloni
CTI Renato Archer, Campinas/SP, Brasil, antonio.balloni@cti.gov.br

Rogério Winter
Unicamp e Exército Brasileiro, Campinas/SP, Brasil

Abstract: We present the gaussian temporal evolution of Corona Virus, the temporal average constant Ktemporal average constant = Kt. The Kt and its standard deviation come from the analysis of 52 experimental gaussian distribution -histogram-. We have analyzed all histograms from 185 countries presented in the reference (Johns Hopkins, 2020), and, we found 52 countries have a definite trend towards an experimental gaussian profile. As a result, we found Kt = K52 countries = (35 ± 5) days - average & standard deviation-. We also calculate using an experimental gaussian got in the reference (Johns Hopkins, 2020), the temporal evolution for the world, the constant Kworld. We found Kworld = Kw = (47 ± ½) days. Finally, up to this date, 20 April/2020, we have only 52 of 185 countries presenting the trends towards an experimental gaussian profile (Johns Hopkins, 2020). The main conclusion from this short communication is that the standard deviation found -Kt = (35 ± 5)days-, is very, which is very good. Therefore, we may conclude the maximum spread of the Corona contamination will occur in a maximum of up to 40 days from the first registered contamination and, in the worst scenario, up to 30 days. Regarding the Brazil peak of contamination, on 10 March/2020, we carried out A PREVISION, and, in that time, we have affirmed by reasoning, the peak in Brazil would be around 10-15 April/2020. Up to this date, there is a confirmation of this prevision. (Johns Hopkins, 2020). For our next prevision, the decrease from contamination must trend to zero among 30-40 days after the peak contamination. These are the most critical situation faced because the real zero takes a while to get to null and, if no personal safety such as social reclusion is adopted, the contamination starts all over.

Keywords: Gaussian Constant K, COVID-19, Temporal Evolution for Constant K, Prevision, Trends, Countries, JHU/CRC

Introduction

This short paper presents the Gaussian temporal evolution from COVID-19, the temporal average constant $\mathbf{K_{temporal\ average\ constant} = K_t}$

The $\mathbf{K_t}$ and its standard deviation come from the analysis of 52 experimental Gaussian distribution -histogram-. The analyses started on April 13, 2020, and concluded on April 20, 2020, when with full analyses from all histograms from 185 countries presented in the reference (Johns Hopkins, 2020). We found 52 countries with a definite trend towards an experimental Gaussian profile -histogram (Johns Hopkins, 2020).

The calculation of **K** for each of the 52 countries followed the methodology presented in figure 1, for Gaussian frequency distribution. Table 1 presents the spreadsheet with all information about each country. The main finding is $\mathbf{K_t} = K_{52\ countries} = (35 \pm 5)$ days, showing the average value and respective standard deviation for those 52 countries.

By using the same methodology presented in figure 1, we also calculated the World temporal evolution constant -$\mathbf{K_{world}}$-. The reference (Johns Hopkins, 2020) makes available the World experimental Gaussian -an histogram-, from where we figured out the $K_{world} = (47 \pm ½)$ days (the "± ½ day" corresponds the half of the column width at the world histogram[1].).

For both calculations of the average $K_{52\ countries}$ and K_{world}, we suppressed the data from several countries because their histogram does not follow and experimental Gaussian profile -histogram (Johns Hopkins, 2020). Finally, up to this date, April 20, 2020, when Table 1 was constructed, we found out -according to our experimental expertise-, only 52 of 185 countries present the trends towards an experimental Gaussian profile -histogram (Johns Hopkins, 2020).

Balloni, A. J., & Winter, R. (2020). The Constant K and The Gaussian Temporal Evolution for COVID-19. In V. M. Bradley & I. Sahin (Eds.), *Proceedings of iLSET 2020-- International Conference on Life Sciences, Engineering and Technology* (pp. 1-5), Washington, DC, USA. ISTES Organization.

The main conclusion from this short paper is that the standard deviation found -see Table 1, $K_t = K_{52\ countries}$ = (35 ± 5) days-, is very low -which is also very good- and this result agrees with the K_{world} = (47 ± ½) days. Therefore, for this analysis, we may conclude -for any Gaussian distribution regarding the Corona Virus contamination-, the maximum spread of the contamination will occur up to, at least, 40 days from the first registered contamination and, in the worst scenario, up to 30 days from the first registered contamination.

By last, regarding the Brazil peak of contamination, we must share that near March 10, 2020, we carried out a prevision -inference-, regarding the peak of contamination in Brazil. In that time, we have affirmed -to our fellows-, by reasoning, and in no formal communication, the peak of COVID-19 contamination in Brazil would be around 10-15 April/2020. That prevision confirmed, according to the Brazilian histogram, presented in (Johns Hopkins, 2020). These previsions were -by inference- carried out by analyzing by several weeks before and up to March 10, 2020, the growing behavior of the contamination for South Korea, China, Italy, and Brazil. This paper proves our preliminary -inference- analyses were entirely right. According to Table 1, the day of minimum point of contamination for Brazil is 9 March 2020, which implies, according to the finding of $\mathbf{K_t}$ of a peak among 9 April 2020 to 19 April 2020 [$\mathbf{K_t} = K_{52\ countries}$ = (35 ± 5) days].

Table 1 shows the 52 unique values for K, collected in the following days: 13 (28 unique values of K), 19 (16 unique values of K), and 20 (8 unique values of K) as of April 2020.

Experimental Calculations of $K_{52\ countries}$ and K_{world}
(Data Source: reference (Johns Hopkins, 2020))

We carried out an extensive analysis from all 185 counties histograms presented in (Johns Hopkins, 2020), and we found 52 countries with a definite trend towards an experimental Gaussian profile -histogram, similar to that theoretical curve of Gauss presented in figure 1-. For each of the 52 countries, we have calculated the **K** value, the temporal distance AB from the first case of contamination (A: MINIMUM) to the peak contamination (B: MAXIMUM), Figure 1.

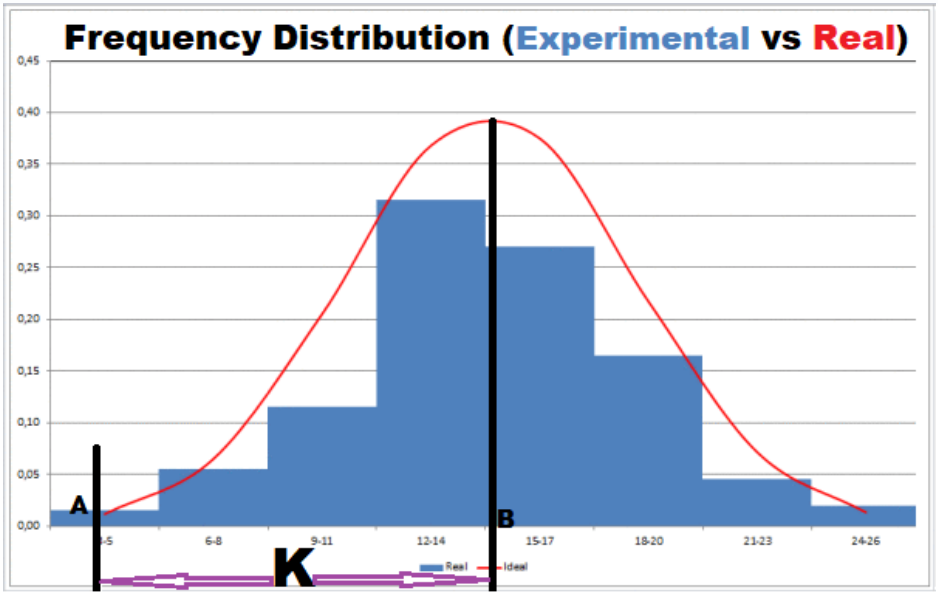

Figure 1. K_{AB} = K is the Constant Temporal Distance -Unique- for a Given Country.
-Source: Authors-

By using an Excel spreadsheet, we have calculated the average value from those 52 **K** -unique value for each country-. Table 1 presents the values found for the **K**, and the average value $\mathbf{K_t}$ as well the respective standard deviation: $K_t = K_{52\ countries}$ = (35 ± 5) days.

Table 1 presents the values of each unique K calculated in Figure 1. The K values presented in Table 1 come from an experimental Gaussian profile, got from reference (Johns Hopkins, 2020). These K's were used to calculate the $\mathbf{K_t}$ -the Average Value of the K's- and the Standard Deviation.

Table 1. The Values of Each Unique K

A	B	D	E	F	G	H
Index	K	Continent	Country	Analysis Day	Start	Peak
1	32	Europe	Armenia	13/04/20	01/03/20	12/04/20
2	30	Europe	Austria	13/04/20	25/02/20	26/03/20
3	39	Asia	Azerbaijan	13/04/20	01/03/20	09/04/20
4	32	Europe	Bosnia and Herzegovina	13/04/20	05/03/20	06/04/20
5	31	Europe	Czechia	13/04/20	29/02/20	31/03/20
6	38	Europe	Denmark	13/04/20	27/02/20	05/04/20
7	36	Europe	Finland	13/04/20	26/02/20	05/04/20
8	37	Europe	Germany	13/04/20	25/02/20	02/04/20
9	37	Europe	Hungary	13/04/20	04/03/20	10/04/20
10	28	Europe	Iceland	13/04/20	28/02/20	27/03/20
11	40	Asia	Iran	13/04/20	19/02/20	30/03/20
12	38	Asia	Iraq	13/04/20	24/02/20	02/04/20
13	36	Europe	Italy	13/04/20	20/02/20	27/03/20
14	35	Europe	Spain	13/04/20	25/02/20	31/03/20
15	42	Asia	South Korea	13/04/20	21/01/20	03/03/20
16	30	Asia	Lebanon	13/04/20	21/02/20	22/03/20
17	34	Europe	Lithuania	13/04/20	28/02/20	02/04/20
18	27	Europe	Luxembourg	13/04/20	29/02/20	27/03/20
19	31	Europe	Malta	13/04/20	07/03/20	07/04/20
20	30	Europe	Norway	13/04/20	26/02/20	27/03/20
21	33	Oceania	New Zealand	13/04/20	28/02/20	01/04/20
22	42	Europe	Sweden	13/04/20	26/02/20	08/04/20
23	30	Europe	Switzerland	13/04/20	25/02/20	26/03/20
24	34	Asia	Taiwan	13/04/20	16/02/20	21/03/20
25	30	Asia	Thailand	13/04/20	25/02/20	26/03/20
26	27	Africa	Tunisia	13/04/20	04/03/20	31/03/20
27	26	Europe Asia	Turkey	13/04/20	16/03/20	11/04/20
28	44	Europe	United Kingdom	13/04/20	26/02/20	10/04/20
29	36	Europe	Greece	19/04/20	26/02/20	02/04/20

I	J	K	L	M	N	O
Index	K	Continent	Country	Analysis Day	Start	Peak
30	27	Oceania	Australia	19/04/20	01/03/20	28/03/20
31	34	America	Canada	19/04/20	07/03/20	10/04/20
32	42	America	Chile	19/04/20	02/03/20	13/04/20
33	36	America	Colombia	19/04/20	06/03/20	11/04/20
34	27	Europe Asia	Cyprus	19/04/20	09/03/20	05/04/20
35	38	Africa Asia	Egypt	19/04/20	11/03/20	18/04/20
36	43	Asia	India	19/04/20	07/03/20	19/04/20
37	37	Europe	Ireland	19/04/20	09/03/20	15/04/20
38	33	Asia	Israel	19/04/20	29/02/20	02/04/20
39	31	Europe	Latvia	19/04/20	02/03/20	02/04/20
40	35	America	Panama	19/04/20	10/03/20	14/04/20
41	32	America	Peru	19/04/20	12/03/20	13/04/20
42	38	Europe	Poland	19/04/20	04/03/20	11/04/20
43	35	Europe	Portugal	19/04/20	02/03/20	06/04/20
44	38	Europe	Romania	19/04/20	04/03/20	11/04/20
45	38	America	Brazil	20/04/20	09/03/20	16/04/20
46	38	America	US	20/04/20	02/03/20	09/04/20
47	39	Europe	France	20/04/20	04/03/20	12/04/20
48	37	Asia	Indonesia	20/04/20	08/03/20	14/04/20
49	33	Europe	Moldova	20/04/20	08/03/20	10/04/20
50	38	Africa	Morocco	20/04/20	10/03/20	17/04/20
51	41	Europe	North Macedonia	20/04/20	06/03/20	16/04/20
52	30	Asia	Uzbekistan	20/04/20	15/03/20	14/04/20

Average	34.90
Standard Deviation	4.73

Regarding Our Next Prevision

We may affirm for those countries following up an experimental Gaussian profile, the DECREASE from CONTAMINATION should trend -have the tendency- **TO ZERO** AMONG minimum of 30 to a maximum of 40 DAYS AFTER THE PEAK CONTAMINATION. These TRENDS are the most critical situation the world is facing because THE ZERO -real zero- takes a while to get to null and, if no proper care -personal safety such as socializing- is adopted, the contamination starts all over again and spreading!

As an example -which supports the above concern-, the graphic presented for South Korea -see daily cases at reference (Johns Hopkins, 2020), and other similar situations for other countries- clarifies the issue. By applying

our $\mathbf{K_t}$ = (35 ± 5) days to the South Korea day of Maximum contamination, i.e., 3 March 2020, we find the following points of Minimum contaminations **[**86 (3 April), 25 (13 April)**]**. However, even after the minimum value (25 contaminations), registered on 13 April 2020, when we should expect for the following days a definitive trend to null -real zero-; this real zero does not occur and, instead, we have the following new contaminations a day after the prevision of the minimum -for the day 13 April 2020-. These news contaminations are shown in the graphic from South Korea (Johns Hopkins, 2020), which presents the following numbers 27, 27, 22, 22, 18, 8, and 13 -where 13 is the number of contaminated as registered on April 20, 2020 (Johns Hopkins, 2020).

Conclusion

We presented a straightforward method applied to a histogram with a Gaussian tendency for calculating the spread of COVID-19 contamination, the constant K. The average value $\mathbf{K_t}$ and its standard deviations [$\mathbf{K_t}$ = (35 ± 5) days] offer a reasonable methodology to easily detect what is ongoing with the temporal spread of COVID-19. From this paper, we conclude the maximum spread of the contamination will occur up to, at least, 40 days from the first registered contamination and, in the worst scenario, up to 30 days from the first registered contamination.

Regarding the Brazil peak of contamination, near March 10, 2020, we predicted -inference-, the peak would be around 10-15 April/2020. We have this confirmation (Johns Hopkins, 2020). Table 1 shows the day of minimum point of contamination for Brazil is March 9, 2020, which implies, according to the finding of $\mathbf{K_t}$ of a peak among April 9, 2020, to April 19, 2020 [$\mathbf{K_t} = K_{52\ countries}$ = (35 ± 5) days].

Our Next Prevision. Similarly, **w**e may affirm for those countries following up an experimental Gaussian profile, the DECREASE from CONTAMINATION should trend -have the tendency- **TO ZERO** AMONG minimum of 30 to a maximum of 40 DAYS AFTER THE PEAK CONTAMINATION. **These TRENDS are the most critical situation the world is facing because THE ZERO -real zero- takes a while to get to null and, if no proper care -personal safety such as socializing- is adopted, the contamination starts all over again and spreading**. See the text of the paper the complete explanation for the country South Korea which is summarized: by applying our $\mathbf{K_t}$ = (35 ± 5) days to the South Korea day of Maximum contamination, i.e., March 3 2020, we find the following points of Minimum contaminations **[**86 (April 3), 25 (April 13)**]**.

However, even after the minimum value (25 contaminations), registered on April 13, 2020, when we should expect for the following days a definitive trend to null -real zero-; this real zero does not occur and, instead, we have the following new contaminations a day after the prevision of the minimum -for the day April 13 2020-. These news contaminations are shown in the graphic from South Korea (Johns Hopkins, 2020), which presents the following numbers 27, 27, 22, 22, 18, 8, and 13 -where 13 is the number of contaminated as registered on April 20, 2020, (Johns Hopkins, 2020). This situation -applying $\mathbf{K_t}$ = (35 ± 5) days to the maximum point of contamination-, could be generalized for any country presenting a histogram with Gaussian distribution.

Recommendations

All over the years, we have had several issues regarding virus contamination. The suggestions are to apply the methodology explained in this short paper to observe if the same trends -previsions carried out in this paper- are valid for those previous virus issues in the world...

Acknowledgment

Dr. Fábio Miranda Pisani, by the understanding of this experimental work and suggestion for improvements and compliance towards innovation and accountability of this paper.

Note

We prepared another version of this paper for publication in the IJonEST Journal. This version has additional secondary information supporting the results presented in the paper published in the iLSet Proceedings. The

paper was submitted for Congress appreciation on April 14, 2020 and has been accepted for presentation, proceedings publication by iLSET, and publication at the journal, IJonEST.

References

Johns Hopkins University of Medicine -Coronavirus Resource Center (2020). Daily Cases, Histograms. Retrieved from *https://coronavirus.jhu.edu/map.html*. Last access on April 20, 2020.

SDFS: A Standardization Technique for Nonparametric Analysis

Avimanyou Kumar Vatsa
Department of Computer Science, Fairleigh Dickinson University, Teaneck, NJ, Unites States, avatsa@fdu.edu

Abstract: Due to availability of computational tools for data acquisition, it is very easy to collect many dimensions from an object. Nevertheless, data acquisition from an object in an experiment may have a low number of dimensions. The analysis of low dimensional data has break-through role. But raw and sparse nature of dataset imposes new challenges and requirements for data analysis due to their special and unique characteristics. In the process of overall characterization of low-dimensional data, the data pre-processing plays crucial role. One of the first processes is normalization and standardization process. Therefore, in this paper, I would like to propose novel standardization technique called SDFS (**S**tandardization for **D**istribution **F**ree **S**tatistics) for nonparametric data analysis. This technique is robust for small sample size with missing values of data points, which commonly exist in real time experiments lead to sparse low-dimensional data. The comprehensive experimental evaluation shows that SDFS standardization is significantly outperforms on existing standardization methods.

Keywords: Low-dimensional, standardization, clustering, nonparametric, sparse dataset

Introduction

In the era of data analysis, the evaluation and analysis of real-world data needs systematic application of statistical and/or logical techniques to unravel and illustrate the knowledge. The techniques required for analysis process depends on the nature of real-world raw dataset. The real-world raw dataset can be gathered from variety of sources and from different applications like research digital photography (Kelly et al., 2015), surveillance videos, field phenotyping and plant phenotyping (Kelly, Vatsa, Mayham, & Kazic, 2015) usually have high or low dimensions.

The analysis of low-dimensional data, with missing data values and small sample size, refer to the possibility of limited amounts of available data and dimensions. The analysis process addresses the many data mining challenges associated with it. These challenges depend on whether data has distribution or not. If it has not any kind of data distribution, it is called nonparametric data analysis. This analysis makes fewer assumptions and are more flexible, robust and applicable to non-quantitative data (Hopkins, Dettori, & Chapman, 2018). But it must need data preprocessing for easier analysis.

Commonly the data preprocessing method includes data cleaning, normalization, transformation, standardization, feature extraction and selection. One of the first steps of data preprocessing is normalization of data because dataset dimensions have different units and scales. So, normalization process makes all dimensions are on same scale and range for fair comparison among them. In this paper, we considered the min-max normalization, a linear transformation, to preserve the behavior of the original data (Han 2012). In general, the min-max normalization uses following formula for range [new_{max_a}, new_{min_a}]:

$$V`_i = (v_i - min_a).(new_{max\_a} - new_{min\_a})/(max_a - min_a) + new_{min\_a}.$$

The next step is data standardization, it is the crucial step of data preprocessing because the variances of the normalized data dimensions are different. Standardization brings all attributes into proportion with one another for fair comparison among them (Standardization, Jajuga 2000, & Milligan, 88). The dimension with large variances tends to have a larger effect on the resulting analysis result than dimension with smaller variances. But the biggest challenge is that there are too many different kinds of standardization methods are available. However, selecting the best standardization method is very dataset dependent. The problem with existing standardization methods is that they are meant for parametric analysis. Therefore, in this paper we are contributing novel standardization method, called Standardization for Distribution Free Statistics (SDFS), for nonparametric analysis (Vatsa 2015; Vatsa 2017). SDFS is really useful for the preprocessing of sparse and small sample size dataset. It has been proven to be plausible way to address the problem of knowledge discovery, optimization, low dimensional data characterization like clustering and other data mining problems.

Vatsa, A. (2020). SDFS: A Standardization Technique for Nonparametric Analysis. In V. M. Bradley & I. Sahin (Eds.), *Proceedings of iLSET 2020-- International Conference on Life Sciences, Engineering and Technology* (pp. 6-9), Washington, DC, USA. ISTES Organization.

The motivation behind this method is the dataset of Dr. Ann Stapleton lab greenhouse experiment. The experiment was designed for maize plants in the greenhouse. The design principle was for ninety different inbred lines (different genetic backgrounds) of plants and forty plants of each line. These plants were treated with nine different growth conditions of nitrogen fertilizer and water. There were four plants under each growth condition except for growth condition five, which had eight plants.

The motivation to know how these nine growth conditions determine the plant phenotype, observable and measurable traits of plant, led to proceed further. Therefore, they measured three prime phenotypes, well observable and measurable of each plant. The phenotypes - plant height, canopy spread, and stem diameter - were measured before and after applying the different growth conditions. Many plants died during the experiment, so the number of surviving plants is often much lower. Nevertheless, this dataset has not any kind of distribution. So, it needs nonparametric analysis for computing optimal growth condition of each inbred lines for each growth condition. Moreover, we were also looking for similar phenotypes among all ninety inbred lines (Vatsa, 2015). But we were not able to solve these two problems because were not able to preprocess the data in right way. Therefore, I proposed SDFS, a novel standardization technique.

The rest of the paper is organized as follows. Sections 2, contain related works of other existing standardization methods. The proposed work is described in section 3. The results and discussion of the proposed technique and comparison with existing techniques are explained in section 4. The scalable feature of proposed techniques discussed in section 5. Finally, our conclusions are given in section 5 and possible future work are also addressed.

Related Work

Walesiak {walesiak90, walesiak99} states that the standardization method is as follows

$$z_{ij} = bx_{ij} + a, (b > 0)$$

where z_{ij} (x_{ij}) denotes the value (standard value) of the j^{th} variable for the i^{th} object. The particular (often used) case of transformation is the one where: $b=1/\sigma$, $a = -\mu/\sigma$
where μ is location parameter and σ is spread or scatter parameter.

This can be written as $z_{ij} = (x_{ij} - \mu)/\sigma$
However, the general existing standardization methods for parametric analysis are given as (stdize)

$$f'(x) = \alpha f(x) + \beta (f \circ g(x))/\gamma$$

where:

- f `(x) is the standardized variates;
- f(x) is the measured attributes;
- α and β are constants;
- f o g(x) shifts the attributes;
- γ is a rescaling function.

γ rescaling functions are hard to choose because the well-known standardization methods consider some descriptive statistics, such as sample mean, sample variance, weighted mean, weighted sum, sum, standard deviation, standard deviation about origin median, Median absolute deviation from median (MAD), Inter quartile range (IQR), range, midrange, Euclidean distance, Biweight one-step M-estimate (Owen 2010), Biweight A-estimate (Owen 2010, Goodall 83, and Kafadar 83} (A-estimators and M-estimators of location are independent of the underlying probability distribution function of the data because they minimize an objective function that is dependent on the distances from the observed values to the estimate. It is similar to Maximum Likelihood Estimators (MLEs)), Huber one-step M-estimate (Bickel 75), Huber A-estimate (Bickel 75, Goodall 83, Iglewicz 83) (These identify robust member of group in asymptotic behavior and has independent identically distributed errors with F distribution symmetric about zero), Wave one-step M-estimate (Iglewicz83), Wave A-estimate \cite{iglewicz83}, AGK estimate (a noniterative univariate form of the estimator) (ACECLUS) (Gnanadesikan 82), Mid-minimum spacing, Minimum spacing and L(p) or Minkowski metric (It is flat space metric used in special relativity. It is combination of Euclidean space and time into a four-dimensional manifold where the space time interval between any two events is independent of the inertial frame of reference in which they are recorded) (Walesiak 99, Jajuga99, Wikipedia).

In our experimental dataset the sample size is very small and so I can't determine its distribution, called nonparametric analysis. Assuming a normal or some other distribution will be hazardous for the data analysis. Therefore, there is need to propose novel standardization technique for nonparametric analysis.

Proposed Standardization, SDFS

In this case the sample size of each combination of lines and growth conditions is too small to test the distribution of the data, so assuming a distribution would be hazardous for data analysis. Therefore, I have proposed a novel method of standardization for the analysis of sparse and non-parametric data:

$f_s(x) = (f(x) - \min f(x))/f(x)$,
where $\$f_s(x)$ represents the value of standardized variates, and f(x) and min f(x) represents measured variates and minimum value of measured variates across groups, respectively.

Results and Discussion

In order to test the effect of proposed standardization techniques, SDFS, we compared SDFS with the other existing standardization techniques like Mean, Median, Sum, Euclen, USTD, STD, Range, Midrange, Maxabs, IQR, MAD, ABW, AHUBER, AWAVE, AGK, Spacing and L. Moreover, according to the experimental results we evaluated SDFS in terms of the data distribution (by Histogram), spatial data representation using three - Dimensional Plots and non-parametric clustering, called MODECLUS, output by three dimensional plots. The detail analysis is included in journal version of this paper.

Effect of SDFS on Clustering

Since clustering is a very useful and popular data characterization method. To observe the effect of this characterization technique we used MODECLUS, a nonparametric clustering algorithm. The clustering performance is also used to evaluate the effect of the standardization technique. This standardization method helps MODECLUS in finding intuitive and natural clusters.

Figure 8, Figure 9, and Figure 10 represent plots of MODECLUS clustering output of standardized values of data points of Δh, Δc, and Δs, which are calculated using standardization methods L, Mean, Median, STD, Euclen, AGK, ABW, AHUBER, AWAVE, IQR, MAD, Maxabs, Sum, USTD, Range, SDFS, Spacing and Midrange. The color of data points shows the cluster number in three dimensional plots. These outcomes are available in journal version of this paper.

Conclusion

Our experimental study show that the proposed method performs completely incomparable to other evaluated techniques. It is superior over existing techniques are due to fact that they assumed that data has some distribution (parametric analysis), while proposed techniques is very useful for data that has not any kind of distribution (nonparametric analysis) and sparse dataset with mixture of positive and negative data values. In contrast to existing standardization techniques, proposed standardization technique (SDFS) does not only aim at characterizing data but also will be used in finding optimization of methods in low dimensional data analysis process. Several questions remain to investigate in our future work like it outperform for univariate data, but we will have to make this for multivariate nonparametric analysis.

Acknowledgment

I sincerely appreciate Dr. Toni Kazic for advice and Dr. Ann Steplton for providing raw dataset of maize phenotype in order to test proposed method. A part of this work was done while I was a graduate student at University of Missouri – Columbia.

References

Bickel, P. J. (1975). One-step huber estimates in the linear model. *J. Am. Stat.* location, in D. C. Hoaglin and Tukey [14], pp. 405–431. *Assoc.*, vol. 70, pp. 428–434.

Goodall, C. (1983). M-estimators of location: An outline of theory, in D. C. Hoaglin and Tukey [14], pp. 339–403.

Han, J., Kamber, M. & Pei, J. (2012). Data Mining Concepts and Techniques: *Cluster Analysis*. Morgan Kaufmann, NewYork. third edition.

Hoaglin, F. M. D. C., & Tukey, J. W. (1983). eds., *Understanding Robust and Exploratory Data Analysis*, (New York), John Wiley and Sons.

Hopkins, S., Dettori, J. R., & Chapman, J. R. (2018). Parametric and Nonparametric Tests in Spine Research: Why Do They Matter? Global Spine J. issue 8(6), pp 652-654, Doi: 10.1177/2192568218782679.

Iglewicz, B. (1986). Robust scale estimators and confidence intervals for location, in D. C. Hoaglin and Tukey [14], pp. 405–431.

Jajuga, K. & Walesiak, M. (2000). Standardization of data set under different measurement scales, *Chapter Classification and Information Processing at the Turn of the Millennium Part of the series Studies in Classification, Data Analysis, and Knowledge Organization*, vol. 1, pp. 105–112.

Kafadar, K. (1982). "The efficiency of the biweight as a robust estimator of location," *J. Research of the National Bureau of Standards*, vol. 88, pp. 105–116.

Kelly, D., Vatsa, A., Mayham, W. & Kazic, T. (2015). Extracting complex phenotypes from images, *Mach. Vision Appl*.

Kelly, D., Vatsa, A., Mayham, W., Ngoˆ, L., Thompson, A., & Kazic, T. (2015). An opinion on imaging challenges in phenotyping field crops, *Mach. Vision Appl*.

Milligan, G. W. & Cooper, M. C. (1988). A study of standardization of variables in cluster analysis, *J. Classification*, vol. 5, pp. 181–204.

NumPy, (Access on 2020). Python - Random Numbers in NumPy: https://www.w3schools.com/python/numpy_random.asp

Owen, M. (2010). *Tukey's Biweight Correlation and the Breakdown (*Master's thesis*)*. Pomona College, California.

Standardization, BioMedWare (2015–present). *methods for standardization.* http://www.biomedware.com/-Methods_for_data_standardization.htm: BioMedWare,.

Stdize, SAS Proc., (2015–present). Http://support.sas.com/documentation/cdl/en/statug/63033/HTML/default/viewer.htm#stdize_toc.htm: SAS(R) 9.4 Functions and CALL Routines: Reference, third ed.

Vatsa, A. (2015). Characterizing Low-Dimensional Phenotypes by Clustering (Master's thesis), University of Missouri – Columbia: https://mospace.umsystem.edu/xmlui/bitstream/handle/10355/47047/research.pdf?sequence=2&isAllowed=y.

Vatsa, A. (2017). An Approach of Clustering Biological Phenotypes (Doctoral dissertation), University of Missouri – Columbia: https://mospace.umsystem.edu/xmlui/handle/10355/62341?show=full.

Wikipedia, Welcome to Wikipedia *(*2020*). The Free Encyclopedia that Anyone Can Edit*. http://en.wikipedia.org/wiki/Main_Page: WikiMedia Foundation.

Ecological Factors Affecting Plant Communities' Distribution on International Tagus River Natural Park

Luís Quinta-Nova
Instituto Politécnico de Castelo Branco. Escola Superior Agrária, Quinta da Sr. de Mércules. 6001-909 Castelo Branco, Portugal, lnova@ipcb.pt

Alice Almeida
Instituto Politécnico de Castelo Branco. Escola Superior Agrária, Quinta da Sr. de Mércules. 6001-909 Castelo Branco, Portugal
Centro de Competências em Cloud Computing (C4-UBI), Universidade da Beira Interior, Rua Marquês d'Ávila e Bolama, 6201-001, Covilhã, Portugal.

João Carvalhinho
Instituto da Conservação da Natureza e das Florestas, I.P., Castelo Branco, Portugal

Abstract: Straddling the frontiers of two neighboring countries around the Tagus River, Portugal and Spain, the International Tagus River Natural Park (ITRNP) extends over an area of 26,484 hectares in the district of Castelo Branco, Portugal. The vegetation of the Park is mainly typical of Mediterranean ecosystems, such as cork oak and holm oak, Mediterranean evergreen scrubland with strawberry tree, kerms oak, terebinth, mock privet, and mastic; thermophilic formations of rockrose, lavender and broom; bush formations, more or less open with olive and wild olive trees; and riparian vegetation, emphasizing the bushweed formations and the galleries of willow trees. In this territory, 726 taxa distributed by 98 botanical families have been identified to date, emphasizing the 51 endemic species detected. In terms of protected Flora the ITRNP the Portuguese endemisms *Festuca duriotagana* and *Linaria amethystea* subsp. *multipunctata*. There are also 41 Iberian endemisms. A study was conducted in the ITRNP to provide insight into the main factors affecting the different plant communities' distribution in the region, and to provide recommendations for the selection of indigenous species in order to monitor the succession process of vegetation in areas affected by wildfires. The study was conducted in sites evenly distributed in the area of ITRNP representing homogeneous vegetation types, the floristic composition and cover of the species were determined in 188 floristic inventories. During the study period, a total of 249 species were recorded. Cluster analysis identified 12 main vegetation communities. The sites were ecologically characterized, at a local scale, using environmental data as bioclimatology, lithology, topography, soil type and its physical and chemical composition. The role of those environmental factors in the explanation of vegetation variation was assessed using canonical correspondence analysis (CCA). Geostatistics tools were also used to interpolate the species distribution and the community diversity index.

Keywords: Plant conservation, Tagus river, protected area, spatial analysis

Introduction

Whether biological communities are deterministic or stochastic assemblages of species has long been a central topic of ecology (Grant & Abbott, 1980; Simberloff, 1981 and Drake, 1990). The widely demonstrated presence of structural patterns in nature may imply the existence of rules that regulate the ecological communities' organization (Colorado, 2015). Drake (1990) suggests that the consequence of the mechanism (e.g., coexistence, extinction, variation in ensemble properties and configurations) appears to be strongly dependent on historical context.

The abiotic environment influences community assembly by restricting which species can be established at the site and by constraining the function of successful colonists (Belyea & Lancaster, 1999; Booth & Swanton, 2002). On the other hand, environmental constraints are assumed to remain constant for long enough that communities approach equilibrium and the outcome of many assembly rules that are resource-based is more likely to be detected (Colorado, 2015). Hence, environmental constraints influence species interactions and the expression of assembly rules related with the availability of space, energy and nutrients (Belyea and Lancaster, 1999).

Quinta-Nova, L., Almeida, A., & Carvalhinho, J. (2020). Ecological Factors Affecting Plant Communities' Distribution on International Tagus River Natural Park. In V. M. Bradley & I. Sahin (Eds.), *Proceedings of iLSET 2020 - International Conference on Life Sciences, Engineering and Technology* (pp. 10-18), Washington, DC, USA. ISTES Organization.

To study the underlying mechanisms driving the assembly of plant species in natural communities is critical for understanding the uneven distribution and the patterns of plant diversity (Gotelli & McCabe, 2002). Among the main deterministic factors, abiotic conditions and plant-plant interactions play crucial roles in determining species co-occurrence and abundance distributions in plant communities. Abiotic variations are well known characteristics which affect plant communities and populations (Khan et al., 2017). These factors contribute to understand distribution, composition and diversity of plant communities (Brown, 1984). Variations in latitude and altitude lead to changes in air temperature, and humidity that then affect the plant species composition and the community structure (Xu et al., 2017).

Daget et al. (1993) refer that the climatic factors that control the vegetation pattern are: global humidity; winter thermal intensity and seasonal thermal contrast (oceanity vs. continentality). Rivas- Martínez (2001) concluded that seasonal thermal contrast is the most important factor that operates in the distribution of vegetation. At a local scale, climate is affected by topography such as slope, elevation and aspect, in addition to affect of evapotranspiration and temperature (Khan et al., 2017).

Temperature and precipitation stand out as the most direct responsible for the distribution of ecosystems on Earth (Rivas-Martínez, 1987). In areas subject to Mediterranean macroclimatic conditions, like the study area, there is always summer aridity with at least two months of drought (Rivas-Martínez, 1996). The water balance is considered as the main conditioning factor for vegetation, and the structure of the Mediterranean vegetation assumes very different types, from closed deciduous or perennial forests, to open forests and scrub, depending on the amount of rainfall available (Costa-Tenorio et al., 1998). In terms of Bioclimatology the study area is under the thermomediterranean thermotype and dry ombrotype conditions.

Soil is also an important ecological limiting factor that determines plant growth, and is influenced by organisms, climate, topography, time and parent material (Hoveizeh, 1997). The Paleozoic substrates are the source of the two main soil units prevalent in the area, the Distric Cambisols and the Eutric Lithosols. The Cambisols appear in the granitic patches and are soils with a high permeability. Lithosols are incipient, without defined horizons, and are dominant in schist areas.

To study the relationships between environmental variables and plant species data researchers use multivariate approaches. The multivariate statistical analytical software assists the ecologists to analyze the effects of environmental factors on different species and to know the structure in the data set (Anderson et al., 2006). The aim of the current study is to identify the main environmental factors that influence the distribution of plant species and communities in the International Tagus River Natural Park (ITRNP) – a protected area that extends over an area of 26,484 hectares in the district of Castelo Branco, Portugal. To provide recommendations for the selection of indigenous species in order to monitor the succession process of vegetation in areas affected by wildfires inside the Natural Park is also an aim of this study.

Method

Site Description

The International Tagus Natural Park is a sanctuary of Nature located in Beira Baixa. Located at the southern end of the county of Castelo Branco and at the south and east end of the county of Idanha-a-Nova, the park corresponds to a strip of approximately 40 km near the river Tagus. The ITNP is an area of recognized importance in terms of nature conservation, for the value it holds for the fauna it contains and the various species strictly protected by international conventions.

The International Tagus Natural Park contains an important faunistic community, including more than two hundred species of vertebrates. The encased valleys of the Tagus and Erges rivers have a wild character that gives them appreciable scenic value. On certain slopes outcrops rise in the form of cliffs forming true rocky gorges like those observed, for example, of the Roman bridge of Segura. So far 179 species of birds have been inventoried in the ITNP. Also identified are 39 species of mammals, 17 species of reptiles, 13 amphibians, 21 fish, and more than 300 species of insects, of which 189 are butterflies. Among the mammals, the presence of the otter, the wild cat and the toad is outstanding.

In this territory, 726 taxa distributed by 98 botanical families have been identified to date, emphasizing the 51 endemic species detected. The ITNP presents communities typical of Mediterranean ecosystems, such as cork oak and holm oak, Mediterranean scrubland with holm oaks, strawberry trees, kerms oak, terebinths, mock privet and mastics, thermophilic formations of rockrose, lavander and broom, bush formations, more or less open with olive and wild olive trees, and vegetation of the lines of water, emphasizing the bushweed formations and the galleries of willow trees.

In terms of Flora, the Lusitanian endemisms *Dittrichia viscosa* subsp. *revoluta*, *Festuca duriotagana* var. *duriotagana*, *Linaria amethystea* subsp. *multipunctata*. There are also 41 Iberian endemisms.

Data Collection and Identification

Data collection took place between 2000 and 2003 and a total of 188 vegetation plots were recorded in all the extension of the territory of the International Tagus Natural Park (see Figure 1). The survey followed the Zurich–Montpellier method (Kent and Coker, 1994).

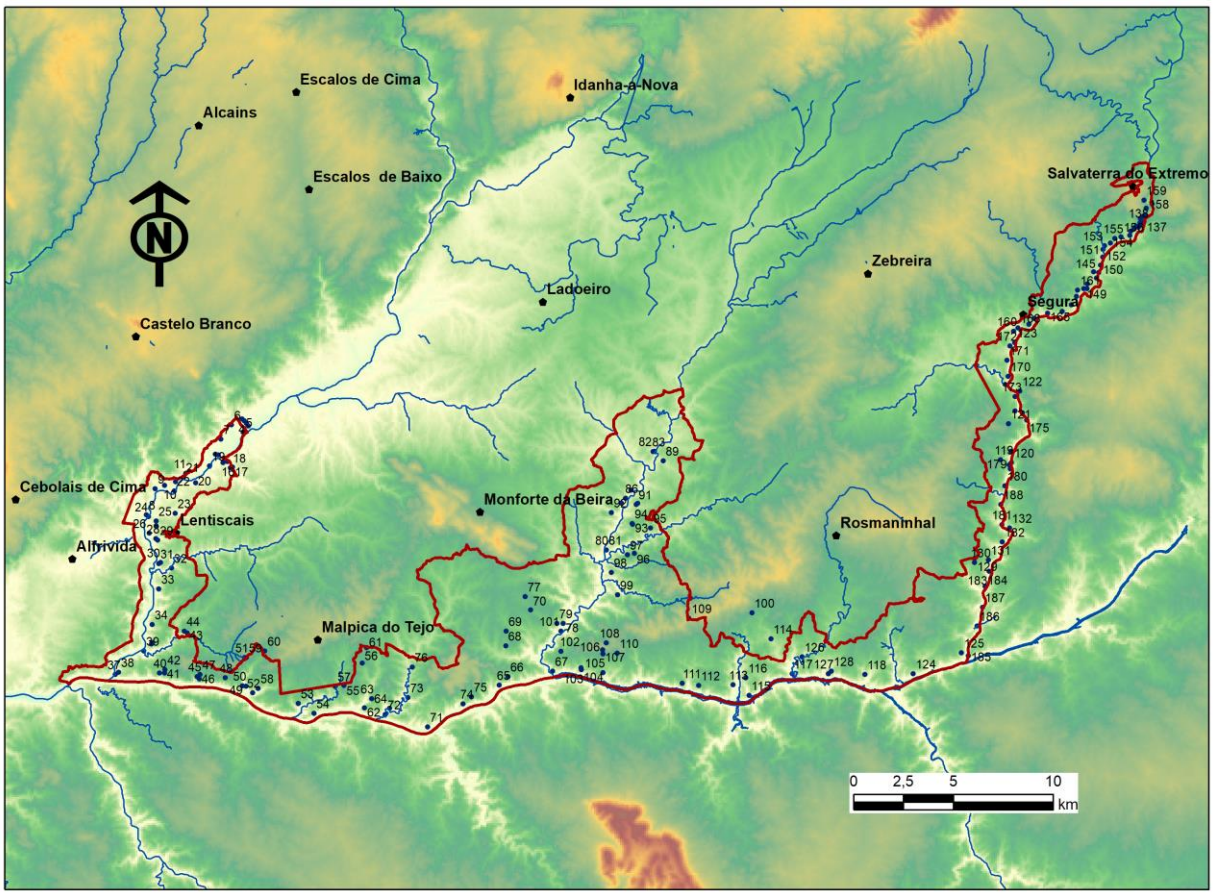

Figure 1. Location of the 188 studied Floristic Inventories

At least were collected 3 individuals of the same taxon, to which were given a code in order to relate with the site of collection. During the collection, was given preference to plants that had a phenology favourable to a correct identification. In laboratory, with the use of optical instruments and plant identification manuals all the collected plants were identified. The concept of minimal area, or the smallest area that represents a community, was applied (Kent & Coker, 1994).

Data Analysis

The obtained data of 188 floristic inventories were arranged in MS Excel for further analyses through Cluster analysis based on abundance classes of the 249 plant species identified.

Cluster analysis UPGMA was used in order to aggregate the main vegetation communities based in its species composition by clustering the sites corresponding to the vegetation plots based on the abundance of plant species.

A GIS data base was loaded with the abundance values of each plant species (249 fields) per sites (188 rows). ArcGIS 10.6 geostatistical tools were used to interpolate the species distribution and the Species Richness. The select method to interpolate a raster surface from a points theme (vegetation plots) was the inverse distance weighted (IDW) technique (Kent & Coker, 1994).

The species data was arranged in columns and sites in rows as per requirement of CANOCO version 5.0 (Šmilauer and Lepš, 2014). The environmental variables data were also arranged in columns and sites in rows in another table. A direct ordination technique - Canonical Correspondence Analysis (CCA) was used to find the influence of different environmental variables in 57 woody plant species presence and abundance.

A diagram was plotted showing the woody species ordered along the canonical axes representing the different environmental factors: Bioclimatology: Thermicity index (It) and Ombrothermic index (Io); Topography: Elevation, Slope and Aspect and Soil types (classification based in soil structure and texture, pH, % OM, % active Ca ($CaCO_3$) and C/N ratio).

Results and Discussion

Distribution Maps

Figure 2 represents the Species Richness distribution raster surface resulting from the interpolation using the inverse distance weighted (IDW) technique from the vegetation plots theme. The highest values of plant diversity are located in the NE part of the ITRNP, along the right bank of the Erges River. To those high Species Diversity values the herbaceous strata contributes strongly.

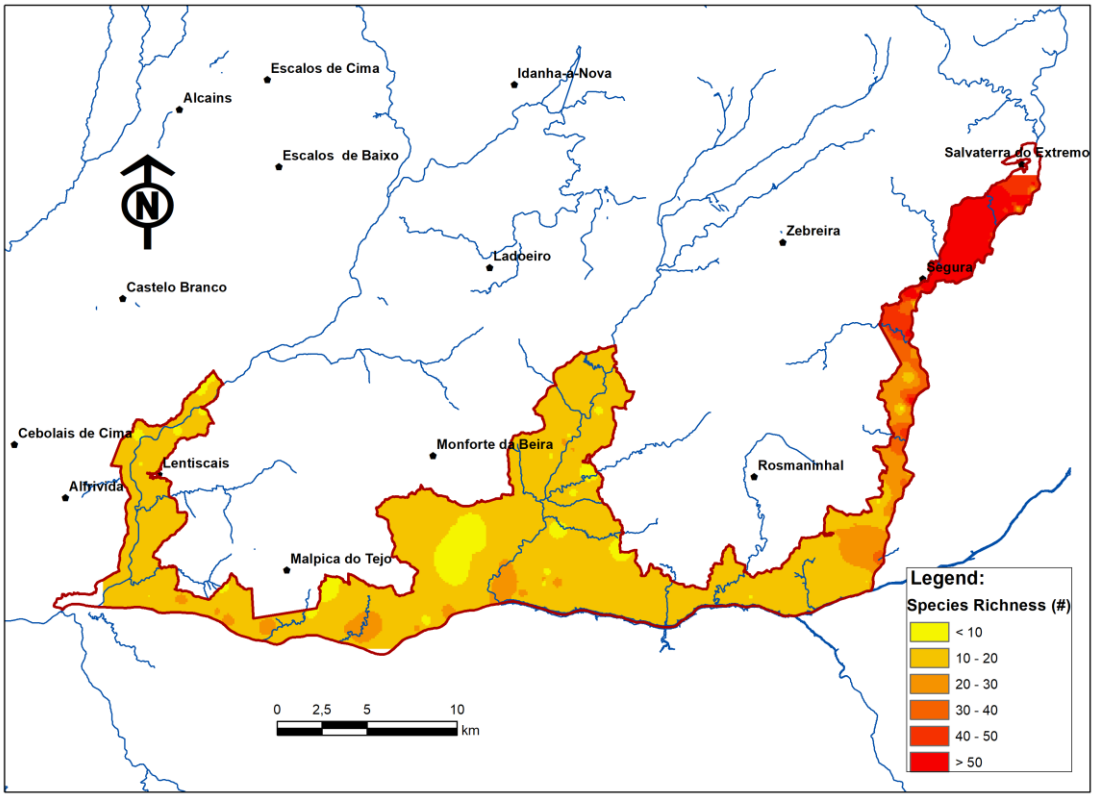

Figure 2. Plant Species Richness

In Figure 3 a) to d) is showed the distribution of four of the most representative woody species, based in the vegetation plots theme, also using the inverse distance weighted (IDW) technique.

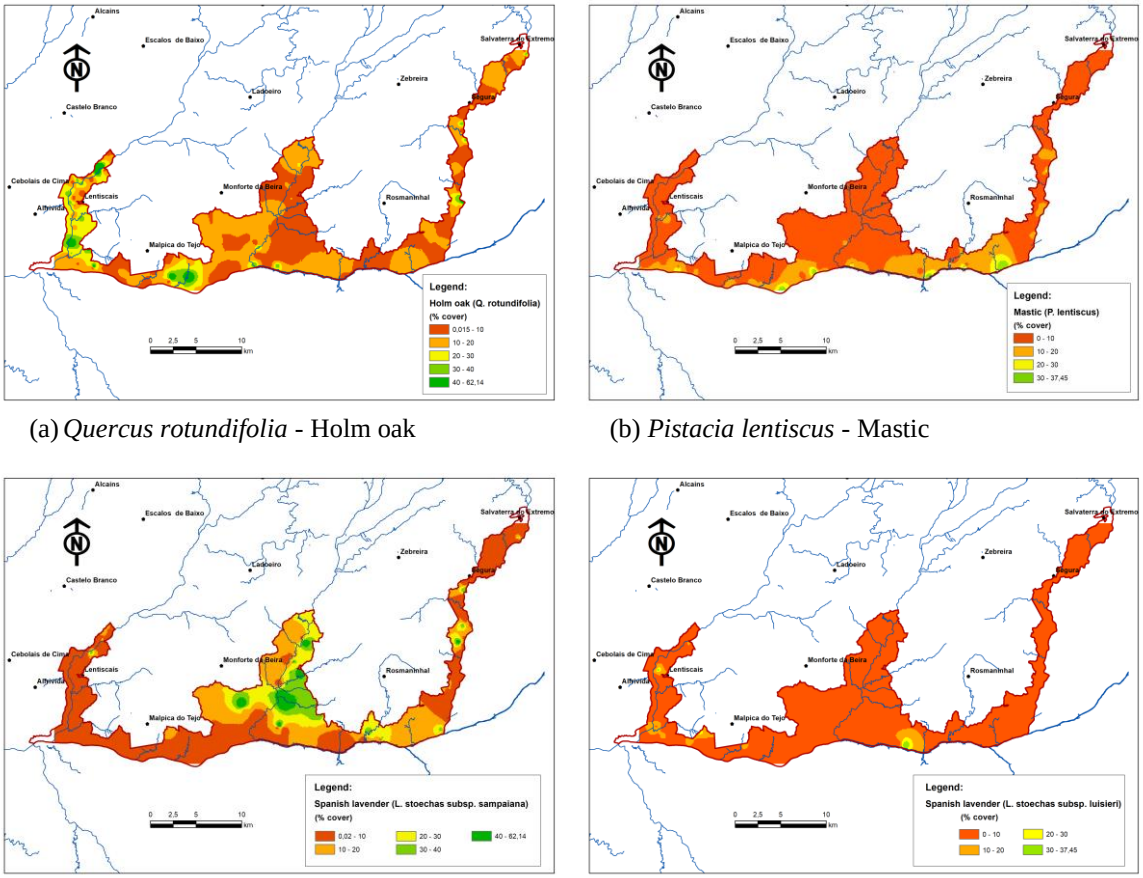

(a) *Quercus rotundifolia* - Holm oak (b) *Pistacia lentiscus* - Mastic

(c) *Lavandula pedunculata* - French lavender (d) *Lavandula stoechas* subsp. *luisieri* - Lavender

Figure 3. Distribution Maps of Some of the Most Representative Woody Species

Cluster Analysis

Cluster analysis established a clear separation of clusters, showed in Figure 4, with five distinctive plant communities identified from the vegetation plots:

Community 1: Different riparian vegetation types - (type 1) dominated by bushweed (*Fluggea tinctoria*), belonging to the community *Pyro bourgaeanae-Securinegetum tinctoriae*; (type 2) dominated by sage-leaved willow (*Salix salvifolia*), belonging to the community *Salicetum lambertiano-salvifoliae*;

Community 2: Natural grassland communities with a high diversity of herbaceous species, belonging to different communities like *Trifolio cherleri–Plantaginetum bellardii*, *Bromo tectorum-Stipetum capensis* and *Phagnalo saxatilis–Rumicetum indurate*;

Community 3: Low density holm oak forest (*Quercus rotundifolia*), belonging to the community *Pyro bourgaeanae-Quercetum rotundifoliae*;

Community 4: Scrubs frequently associated to low density holm oak areas, dominated by gum rockrose (*Cistus ladanifer*), belonging to the community *Genisto hirsutae-Cistetum ladaniferi*;

Community 5: Tall scrubs dominated by species like retama broom (*Lygos sphareocarpa*) and Portuguese broom (*Cytisus striatus*), belonging to the community *Cytiso multiflori-Retametum sphaerocarpae*.

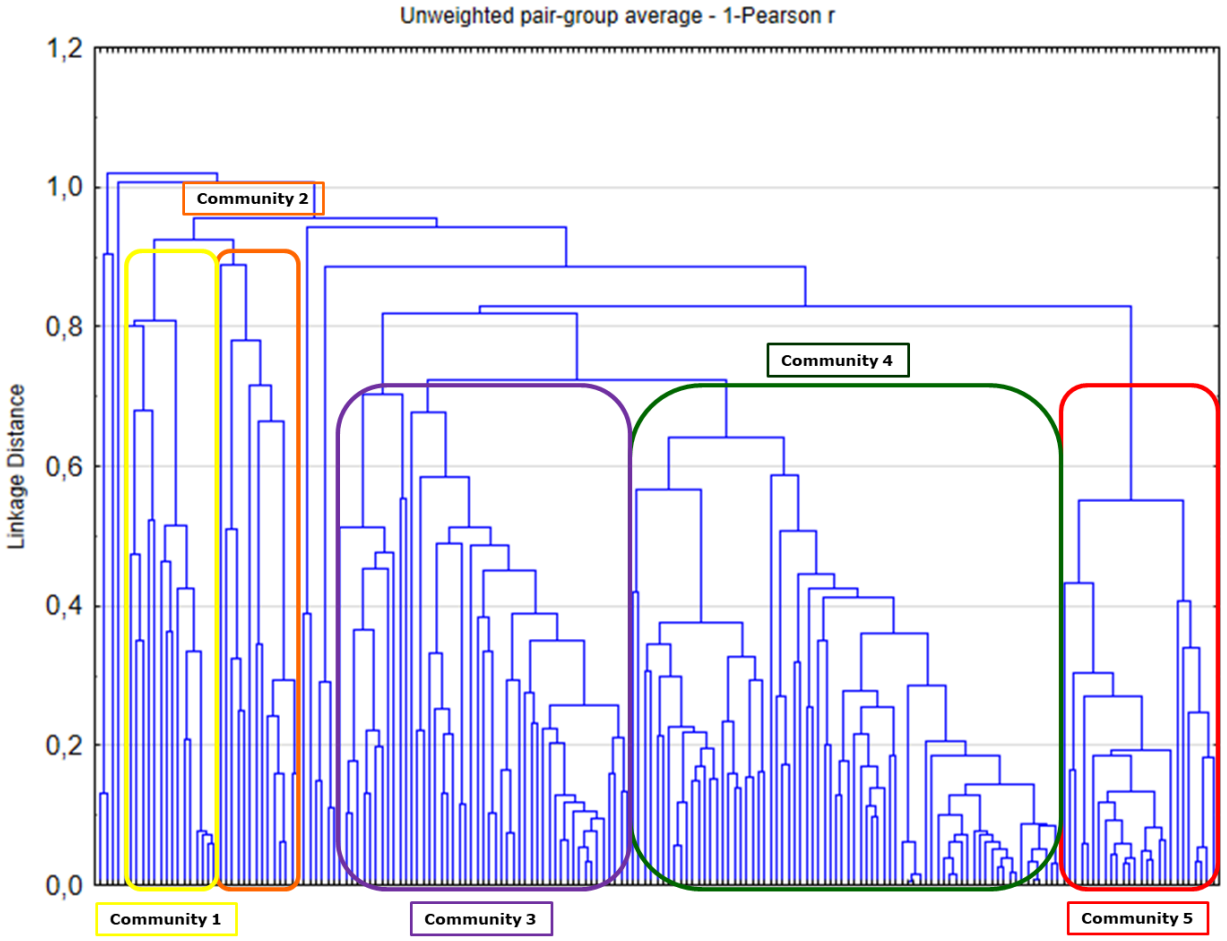

Figure 4. Cluster Dendrogram of 188 Plots Showing Plant Communities

Canonical Correspondence Analysis

The Monte Carlo permutation test showed that there was a significant correlation (P=0.002) between the five environmental variables and the ordination axes. The cumulative variance explained with the first two axes is 71,29% (Table 1).

Table 1. CCA Summary Table

Statistic	Axis 1	Axis 2	Axis 3	Axis 4
Eigenvalues	0.2709	0.1964	0.0912	0.0576
Explained variation (cumulative)	4.95	8.54	10.21	11.26
Pseudo-canonical correlation	0.7142	0.7398	0.6039	0.5355
Explained fitted variation (cumulative)	41.33	71.29	85.21	93.99

Through the interpretation of the explanatory variables axes of the CCA Biplot (Figure 5) it can be seen that the first axis is positively correlated with the Bioclimatology and Soil type. The variables that are positively correlated with the second axis are the topographic ones - Elevation and Aspect. In Table 2 are presented the legend of the plant species abbreviations. The most important environmental factors affecting the abundance of plant species in the ITRNP area were slope, elevation and soil type.

Species more commonly associated with high altitude areas furthest from the Tagus River include shrub species like *Chamaespartium tridentatum*, *Genista hirsuta* and *Genista triacanthos*. In steep areas the plant species more adapted to those conditions are *Arbutus unedo*, *Viburnum tinus* and *Cistus populifolius*.

The main parameter that separates species correlated with the environmental factor Soil type is the soil moisture. The plant species positively correlated with the Soil type have as habitat areas with high soil moisture located in river banks - riparian vegetation, like *Fluggea tinctoria*, *Alnus glutinosa*, *Fraxinus angustifolia*, *Salix salvifolia* and *Rubus ulmifolius*. The plant species negatively correlated with Soil type are associated to dryer soils like *Quercus rotundifolia* and *Olea europaea*.

In summary, CCA ordinations suggest that there are statistically significant relationships between plant species distributions and the selected environmental variables.

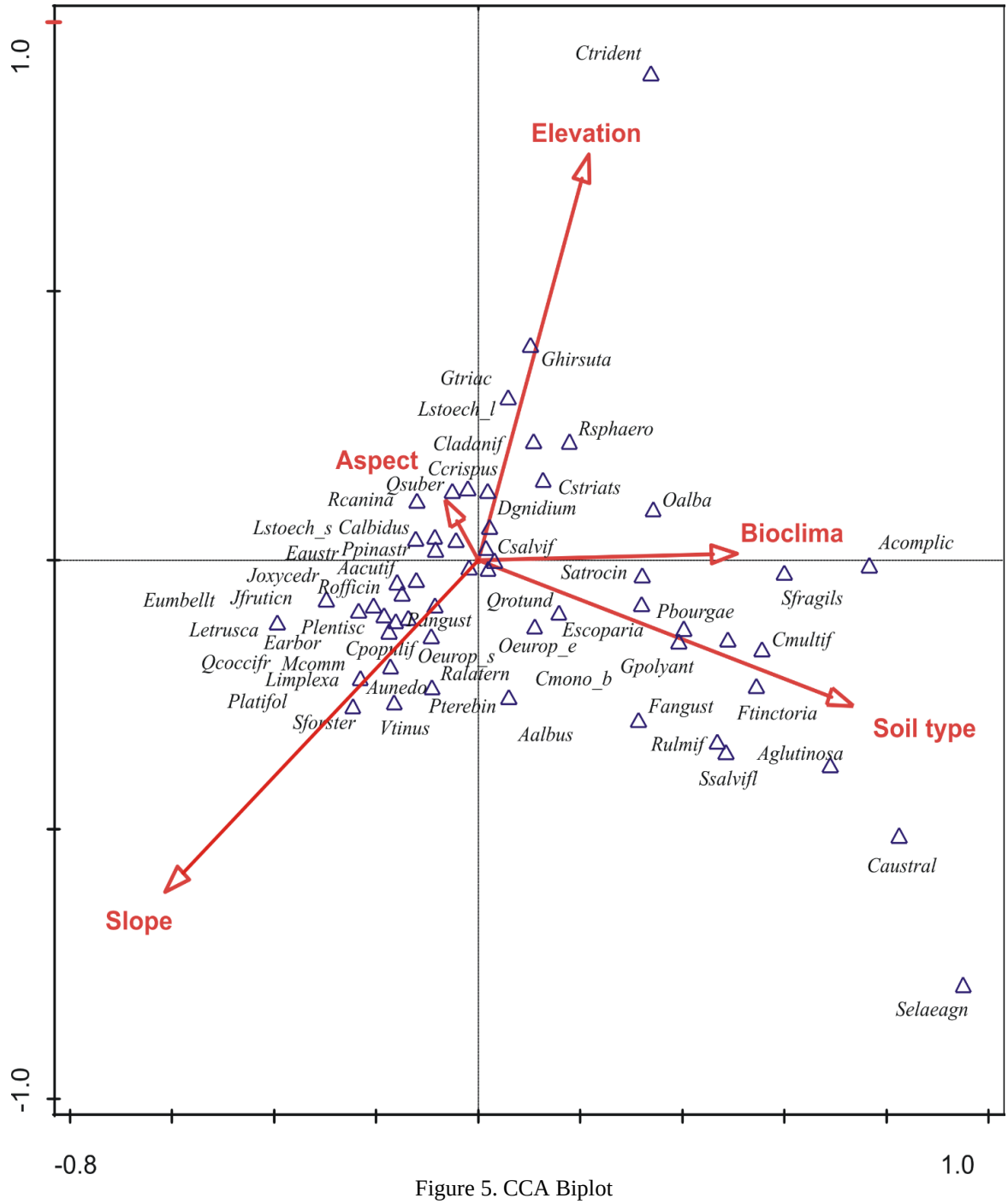

Figure 5. CCA Biplot

Table 2. Species Abbreviation used in CCA Biplot

Abbrev.	Scientific name	Abbrev.	Scientific name	Abbrev.	Scientific name
Aacutif	*Asparagus acutifolius*	Fangust	Fraxinus angustifolia	Platifolia	*Phillyrea latifolia*
Aalbus	*Asparagus albus*	Ftinctoria	Fluggea tinctoria	Plentiscus	*Pistacia lentiscus*
Acomplic_a	*Adenocarpus complicatus*	Ghirsuta	Genista hirsuta	Ppinaster	*Pinus pinaster*
Aglutinosa	*Alnus glutinosa*	Gpolyanth	Genista polyanthos	Pterebin	*Pistacia terebinthus*
Aunedo	*Arbutus unedo*	Gtriac	Genista triacanthos	Qcoccifera	*Quercus coccifera*
Caustralis	*Celtis australis*	Hocym	Halimium ocymoides	Qrotund	Quercus rotundifolia
Calbidus	*Cistus albidus*	Hviscosum	Halimium viscosum	Qsuber	Quercus suber
Ccrispus	*Cistus crispus*	Jfruticans	Jasminum fruticans	Ralaternus	Rhamnus alaternus
Cladanifer	*Cistus ladanifer*	Joxycedrus	Juniperus oxycedrus subsp. oxycedrus	Rcanina	Rosa canina
Cmono_b	*Crataegus monogyna* subsp. *brevispina*	Letrusca	*Lonicera etrusca*	Rofficin	Rosmarinus officinalis
Cmultif	*Cytisus multiflorus*	Limplexa	*Lonicera implexa*	Roleoides_f	Rhamnus oleoides subsp. fontqueri
Cpopulif	*Cistus populifolius*	Lstoechas_l	*Lavandula stoechas* subsp. *luisieri*	Rsphaero	Retama sphaerocarpa
Csalvif	*Cistus salvifolius*	Lstoechas_s	*Lavandula pedunculata*	Rulmif	Rubus ulmifolius
Cstriatus	*Cytisus striatus*	Mcomm	*Myrtus communis*	Satrocine	Salix atricinerea
Ctrident	*Chamaespartium tridentatum*	Oalba	*Osyris alba*	Selaeagnos	Salix elaeagnos
Dgnidium	Daphne gnidium	Oeurop_eur	*Olea europaea* var. *europaea*	Sforsteranum	Salix forsteranum
Earbor	Erica arborea	Oeurop_syl	*Olea europaea* var. *sylvestris*	Sfragilis	Salix fragilis
Eaustr	Erica australis	Pangust	*Phillyrea angustifolia*	Ssalvifolia	Salix salvifolia
Escopar_s	Erica scoparia subsp. scoparia	Pbourgae	*Pyrus bourgaeana*	Vtinus	Viburnum tinus
Eumbellata	Erica umbellata				

Conclusion

Primarily, this study will improve the understanding of the distribution and ecology of plant taxa in the International Tagus River Natural Park, and its results provide data that can be used as a baseline for monitoring change. The study results will be helpful to stakeholders in order to manage the natural and agroforest production areas inside the Natural Park and to provide recommendations for the selection of indigenous species in order to monitor the succession process of vegetation in areas affected by wildfires.

The combination of multivariate analysis and GIS gave important insights. The Cluster Analysis exposed five vegetation types, and can therefore be seen as useful tools in vegetation ecology studies. The CCA reveal that the environmental factor Slope, Elevation and Soil type are the most influential factors that explain the species distribution in ITRNP.

Recommendations

Further study on the factors that influence the distribution of plant species in ITRNP and the possible effects of climate change on the distribution patterns is needed.

Acknowledgements

This work was carried out in the aim of the "WP2.7 - Bioclimatic modelling, landscape structure, biodiversity and climate change" of the C4 - Cloud Computing Competence Center, Beira Interior University; and is financed by national funds through FCT - Foundation for Science and Technology, under the project UIDB / 00681/2020.

References

Anderson, M. J., Ellingsen, K. E., & McArdle, B. H. (2006). Multivariate dispersion as a measure of beta diversity. *Ecol. Lett*. 9, 683–693.

Belyea, L. R., & Lancaster, J. (1999). Assembly Rules within a Contingent Ecology. *Oikos*, 86, 402-416.

Booth, B., & Swanton, C. (2002). Assembly theory applied to weed communities. *Weed Science*, 50(1), 2-13.

Brown, J. H. (1984). On the relationship between abundance and distribution of species. *Am. Nat.*, 255–279.

Colorado, G. J. (2015). How ecological communities are structured: a review on ecological assembly rules. *Revista EIA*, (24), 27-53.

Costa-Tenorio, M., Morla-Juaristi, C., & Sainz-Ollero, H. (1998). *Los bosques ibéricos: Una interpretación geobotánica*. Editorial Planeta, Barcelona.

Daget, P., Adhali, L., & David, P. (1993). Vegetation, nutrition and climate - examples of integration: mediterranean bioclimate and its variation in the paleartic region. *Repères* 5.

Drake, J. A. (1990). Communities as assembled structures: do rules govern patterns. *Trends Ecol. Evol.* 5, 159-164.

Gotelli, N., & McCabe, D. (2002). Species Co-Occurrence: A Meta-Analysis of J. M. Diamond's Assembly Rules Model. *Ecology*, 83(8), 2091-2096.

Grant, P. R., & Abbott, I. (1980). Interspecific competition, island biogeography and null hypotheses. *Evolution* 34, 332-341.

Hoveizeh, H. (1997). Study of the vegetation cover and ecological characteristics in saline habitats of Hoor-e-Shadegan. *J. Res. Constr*. 34, 27-31.

Kent, M., & Coker, P. (1994). Vegetation Description and Analysis. Vegetation Description and Analysis: A Practical Approach. John Wiley and Sons, Chichester.

Khan, M., Khan, S. M., Ilyas, M., Alqarawi, A. A., Ahmad, Z., & Abd Allah, E. F. (2017). Plant species and communities assessment in interaction with edaphic and topographic factors; an ecological study of the mount Eelum District Swat, Pakistan. *Saudi journal of biological sciences*, 24(4), 778–786.

Rivas-Martínez, S. (1987). *Memoria del Mapa de las Séries de Vegetación de España a escala 1:400.000*. ICONA - Série Técnica, Madrid.

Rivas-Martínez, S. (1996). *Geobotánica y Bioclimatologia*. Discurso de Doctor "Honoris Causa" de la Universidad de Granada. http://www.globalbioclimatics.org.

Rivas-Martínez, S. (2001). Vegetação da Europa Mediterrânica: bioclimatologia, zonamento e vegetação potencial. *2.º Curso Avançado de Fitossociologia*. Fédération Internacional de Phytosociologie, ISA, Lisboa.

Simberloff, D. (1981). Community effects of introduced species. In: Nitecki MH (ed) *Biotic Crises in Ecological and Evolutionary Time*, pp 53–81. Academic Press, New York.

Šmilauer, P., & Lepš, J. (2014). *Multivariate Analysis of Ecological Data using CANOCO 5* (2nd ed.). Cambridge: Cambridge University Press.

Xu, M., Ma, L., Jia, Y., & Liu, M. (2017). Integrating the effects of latitude and altitude on the spatial differentiation of plant community diversity in a mountainous ecosystem in China. *PLoS ONE* 12(3): e0174231.

Analysis and Comparison of the Meaning of Waves in Physics, Mathematics, Music, Fine Arts, Everyday Life

Goranka Stanić
Škola Primijenje Umjetnosti, Croatia, goranka.stanic@gmail.com

Abstract: When we mention the word "wave", we connect it with the natural sciences, physics. Physics is a science that explains all phenomena in our micro and macro environment. Although we have learned a lot of data, laws, new surprises and discoveries are still being made. Science is directly related to all areas of our lives. In my work, I made a comparison of the physical phenomenon "wave" which is in various ways associated with mathematics, music, speech, and fine arts. A wave is the propagation of a disturbance by which energy is transmitted through a medium without the medium as a whole moving. When waves are found at the boundary between two different means, their deflection, refraction or reflection (repulsion) occurs and, under special conditions, standing waves. Mechanical waves can propagate only through a substance (medium), while electromagnetic waves can also propagate in a vacuum. The basic division of waves can be classified according to several rules. One of them is the division into transferal, longitudinal and standing wave. Periodic waves can be described by characteristic quantities: frequency, amplitude, period, and wavelength. The depressions that occur when we throw the agent into the water are called wave valleys, and the protrusions are called wave ridges, and in the case of transfer wave waves, the ridges are areas of higher density, and the valleys of rarer density.

Keywords: Waves, mathematic, physic, art, music, everyday life

Introduction

The basic division of waves can be classified according to several rules. One of them is the division into transferal, longitudinal and standing wave. Periodic waves can be described by characteristic quantities: frequency, amplitude, period, and wavelength. The depressions that occur when we throw the agent into the water are called wave valleys, and the protrusions are called wave ridges, and in the case of transfer wave waves, the ridges are areas of higher density, and the valleys of rarer density.

Waves are described by: wavelength λ ,, distance between two banks or valleys of a sinusoidal wave; the period of the wave T, the time elapsed as the wave shifts by one wavelength; wave number k, the magnitude of the reciprocal wavelength, and ffrequency f, the magnitude of the reciprocal period. Waves propagate in space at a certain speed called the speed of wave propagation. During one period, during T in which the particle in the wave source performed one complete oscillation, the oscillation shifted by the wavelength λ.

In the field of physics, we distinguish between mechanical waves, electromagnetic waves, harmonic waves, surface and spatial waves, standing waves, matter waves, gravitational waves. I compared the properties of waves in different branches, physics, electromagnetic waves, sound waves. Wavelength: in a sound, mechanical wave determines the pitch. In fine art, tone is associated with the characteristic brightness in color or achromatic scale, or shade. Tone in musical art is marked by note, octave, pitch, and place on the musical scale. The intensity of the wave is in the musical volume, in the fine arts purity and colors.

Harmony is the proper oscillation or alternation of valleys and ridges in a classical mechanical wave, in fine art there is talk of harmony of colors and shapes, and musical art of a major that is cheerful, pleasant, veso, or mole, which though harmonious sounds sad. Contrary to harmony is noise in the art of music, these are special relationships of notes that do not evoke the atmosphere of the ear, in the art of music we translate it as impure color, and in everyday sounds as impure sound that is vaguely heard, and rustles.

Rhythm in any physical form of wave observation is the alternation of valleys and ridges, which can be regular or irregular, faster or slower. He plays an important role in the art of music, as well as in fine art. Color is primarily related to the field of art and we distinguish between primary and secondary colors, while the same terminology in music art is used for various instruments and sound that characterizes a particular wave source.

Stanić, G. (2020). Analysis and Comparison of the Meaning of Waves in Physics, Mathematics, Music, Fine Arts, Everyday Life. In V. M. Bradley & I. Sahin (Eds.), *Proceedings of iLSET 2020-- International Conference on Life Sciences, Engineering and Technology* (pp. 19-25), Washington, DC, USA. ISTES Organization.

The mathematical wave is closely related to the sinusoid, and thus to the circle and circular motion. The circle in art occupies a special place as a proper form, or composition. Physics is a fundamental natural science that deals with materials, motion, energy, and interaction. Physical laws are expressed in mathematical form.

Physics and mathematics are intertwined in many ways, so that the non-existence of only one of them would be impossible Mathematics is an exact science that studies axiomatically defined abstract structures using mathematical logic. Art is the totality of human spiritual activity by which an aesthetic experience is created, including the work created and the experience of the work.

Waves

When we mention the word "wave" we associate it with the natural science of physics. Physics is a science that explains everything intensified in our micro and macro environment. Even though we learned a lot of data, laws, we still realized new surprises and discovered. A science is directly related to all environments of our lives.

A wave is the propagation of a disorder that transmits energy through some medium, and this medium as a whole does not move. The basic division of waves can be classified according to several rules. One of them is the division into transverse, longitudinal and standing wave.

Waves are described by: wavelength λ „ distance between two banks or valleys of a sinusoidal wave; the period of the wave T, the time elapsed as the wave shifts by one wavelength; wave number k, the magnitude of the reciprocal wavelength, and frequency f, the magnitude of the mutual period. Waves propagate in space uncomplicatedly fast which is called the speed of wave propagation. During one period, to the joke during T in which the particle at the source of the wave made one complete oscillation, the oscillation shifted by the wavelength λ.

Hormones are interrelated by mathematical ratios (integers) of frequency codes musical instruments. Flickering wire or rodhe appears a sinusoidal wave of displacement, and after reflection at the ends of the rod sinusoidal standing waves are formed. The way this addict will be about it will be his ends loose or fixed.

Music is an art that rarely consists of sound wavy frequencies that appear in turn copies. It consists of tones, and the distances in height between any two tones are called intervals. Sound quality is a characteristic that distinguishes the ways in which sound is produced, such as voice or music instrument - stringed instruments, wind instruments or percussion. Sound quality and color are determined in the form of a sound wave, and they also depend on the number and type and representation of higher frequencies. What is it the higher the tone frequency, the higher the pitch.

Wavelength

Physics

Wavelength (sign λ), the shortest distance between two points of a medium that vibrate in the same phase when a wave propagates through a medium. It can also be described as the distance for which the wave propagates during one period T, ie: $\lambda = vT$ and as the quotient of the speed of propagation of the wave v and its frequency f, therefore: $\lambda = v / f$. The wavelength is the distance between adjacent wave particles that are at the same distance from the equilibrium position and move in the same direction.

Mathematics

$y = a \sin (bx + c)$ using different values for a, b, and c. b is the period of the sine curve.

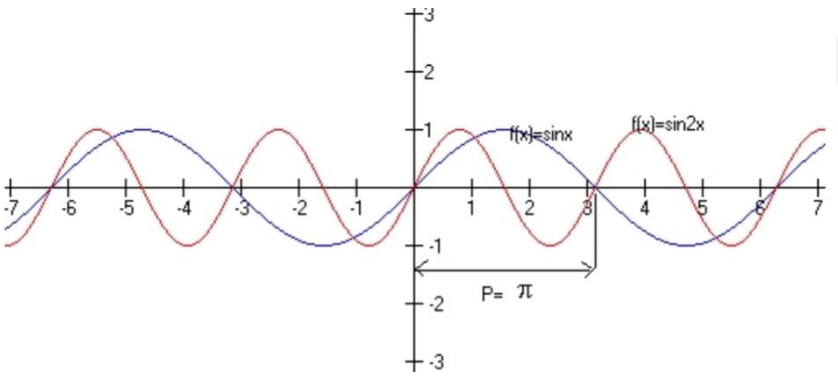

Figure 1. Sinusoids and Wavelengths

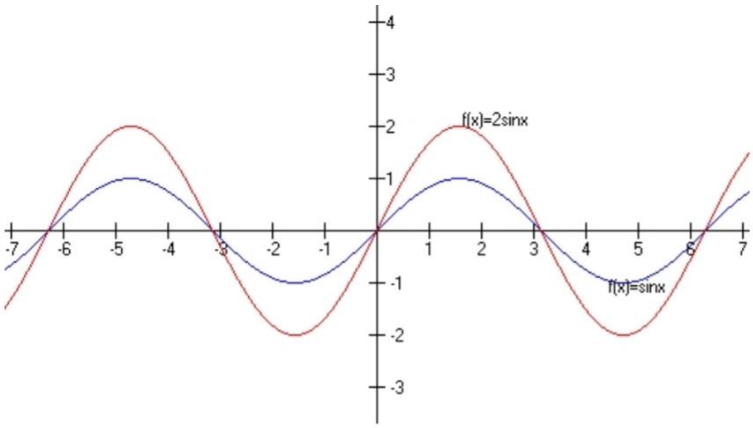

Figure 2. Sinusoid and Amplitude

Fine Arts

The human eye is sensitive only a small part of it spectrum, to the visible part spectrum, the so-called white light (approx. 380 - 750 nm). The wavelength of visible light that we experience as colors is between 400nm, purple, up to 700nm red

Frequency

Mathematic

Mathematics - via the sinusoid equation - wavelength period - we connect it with the period if we replace the x axis in the sinusoid with the time t in the physical notation.

Period equation:
f(x) = a sin(bx + c)
a is amplitude. The largest and smallest value that the function can take

Physics

Wave equation:
$y = A\sin\left[\frac{2\pi}{T}\left(t - \frac{x}{v}\right)\right]$

Art

Frequency is related to the physical aspect of electromagnetic radiation in fine arts. If we look at frequency as the number of vibrations per minute, we experience it as an artistic element of the composition rhythm. In an artistic composition, each alternation of elements is defined as rhythm (light dark, round, sharp, lines, dots, lines of alternation of colors, etc.). The art of music uses frequency to create harmonic tones, and music

Speed

Physics

Different waves of different speeds

$v=f\lambda$

Music

Tempo is the speed of a song. It can be fast (presto, vivo, allegro), moderate (allegretto, moderato, andante) and slow (adagio, lento, largo)

Harmony

Physics

Harmonic vibration, the vibration of a body or particle under the action of a harmonic force. a s (t) ≡ s elongation or displacement of the body from an equilibrium position.

Music

Harmony is music is a term that appears from ancient to modern writers in different meanings: as a synonym for music and melody, as a name for a tonal system, tonal gender or for an octave range, or for a type of scale, and as a sign for polyphony and finally as a consonant label. – In a narrower sense, harmony is understood as a chord, ie vertical structure of musical works

Linguistics

In linguistics, the most common type of harmony is vocal (vowel) harmony, as it exists in the Uralic languages (eg Hungarian) or the Turkish language (eg Turkish).

Intensity

Physics

Strength (intensity), a measure of the effect of physical action, is part of the name of many physical In order not to be repeated in a large number of names, in modern metrological norms, wherever necessary, the word strength is omitted (eg electric current is called only electric current).

Fine Arts

We equate intensity in painting with the purity of color and the density of pigment.

Music

Intensity is an integral part of music and in musical notation is denoted by the two basic dynamic indications in music are: p or piano, meaning "soft" , or forte, meaning "loud or strong"

Tone

Music

A complex sound that is created by regular and periodic vibrations of the air, and its partial tones are in the most harmonious relationship and therefore we can precisely determine the so-called. bias. Tone, unlike sound in the narrower sense of the word (whose partial tones are less harmonious and the pitch less unambiguous), is traditionally considered a basic element of music. It is closely related to the material and structure of a musical instrument

Linguistics

Prosodic element consisting of variations of tone (high, middle, low tone) and melody (ascending, descending, etc. line) and usually, in a particular language, affects the whole syllable.

Art

The name for the property and shade of color; the colors act warmer if they are deeper and more saturated, and cooler if mixed with white pigment. By mixing more than two spectral colors, midtones are obtained. Tonal painting achieves the plasticity of form and the illusion of spatiality achieved with a linear perspective and chiaroscuro.

Music

A tone is a sound that has a certain pitch, volume, duration, and color, which distinguishes it from other, indeterminate sounds (such as noises). Its properties are determined by the physical values of the sound waves from which it originates. The height depends on the frequency of the sound wave. The higher the frequency of the tone, the "higher" the human hearing will perceive. The strength depends on the amplitude of the wave. Higher amplitude vibrations also produce a stronger tone. The duration depends on the time of the sound wave transmission. The tone lasts as the sound source produces vibrations.

Color

Physics

The eye receives the reflected light from the object, this light signal is converted into a nerve, which is transmitted through the nerves to the brain and there is a sense of color. The sensation of color in our eye causes electromagnetic radiation of wavelengths 380 - 750 nm.

Art

In our eyes, Oja called photosensitive reaction cones to an external stimulus in the form of light rays. Entering the eyes, the air is refracted as in a prism and scattered into the spectrum. While all the colors of the spectrum are united, the ray is white - that is why we call white colorless, uncolored or achromatic. Achromatic are both black and gray.

Spectrum (lat. Spectrum - spirit, representation) was discovered by Isaac Newton1676 Redirecting white light into a three-sided prism, he saw that all existing colors were hidden in it. An endless array of overflowing colors makes it the final distinction of seven different colors: red, orange, yellow, green, cyan (light blue), indigo (dark blue), and purple. He took the number seven for correlative (and esoteric) reasons - so that seven colors would correspond to seven notes in the musical scale.

Color is the perception of a certain frequency range (vibration) from 400 to 800 trillion Hz. Before red, it is invisible infrared, and after purple invisible ultraviolet. The color we see not in the spectrum is magenta (purple); it is the interference (overlap) of waves.

Music

Color, which depends on the means by which musical works are performed, i.e. on the human voice or on the type of instrument; form, ie a sound whole based on the most diverse possibilities of exposure, mutual combination, variation, sequence or elaboration of tonal structure - sound elements. The basic features of the voice are: volume, pitch and color.

Method

Many years of work in the fields of mathematics, physics, music, and fine arts have led to an analysis of the notion of the “wave” that connects these branches. Comparison, analysis, and deductions and inductions have explained and highlighted the connection among the many aspects of human reality in which we live and is encompassed by waves.

Results and Discussion

In addition to the concepts and analysis announced in the summary, I have dealt in even more detail with the role, the similarity of “wave” terminology in various fields of science, art, and everyday life. Waves are described by: wavelength λ ,, distance between two banks or valleys of a sinusoidal wave; the period of the wave T, the time elapsed as the wave shifts by one wavelength; wave number k, the magnitude of the reciprocal wavelength, and frequency f, the magnitude of the reciprocal period. Waves propagate in space at a certain speed called the speed of wave propagation. During one period, during T in which the particle in the wave source performed one complete oscillation, the oscillation shifted by the wavelength λ.

In the field of physics, we distinguish between mechanical waves, electromagnetic waves, harmonic waves, surface and spatial waves, standing waves, matter waves, gravitational waves. I compared the properties of waves in different branches, physics, electromagnetic waves, sound waves.

Wavelength: in a sound, mechanical wave determines the pitch. In fine art, tone is associated with the characteristic brightness in color or achromatic scale, or shade. Tone in musical art is marked by note, octave, pitch, and place on the musical scale. The intensity of the wave is in the musical volume, in the fine arts purity, and colors.

Harmony is the proper oscillation or alternation of valleys and ridges in a classical mechanical wave, in fine art there is talk of harmony of colors and shapes, and musical art of a major that is cheerful, pleasant, veso, or mole, which though harmonious sounds sad. Contrary to harmony is noise in the art of music, these are special relationships of notes that do not evoke the atmosphere of the ear, in the art of music we translate it as impure color, and in everyday sounds as impure sound that is vaguely heard, and rustles.

Rhythm in any physical form of wave observation is the alternation of valleys and ridges, which can be regular or irregular, faster or slower. He plays an important role in the art of music, as well as in fine art. Color is primarily related to the field of art and we distinguish between primary and secondary colors, while the same terminology in music art is used for various instruments and sound that characterizes a particular wave source. The mathematical wave is closely related to the sinusoid, and thus to the circle and circular motion. The circle in art occupies a special place as a proper form, or composition.

References

Brüel & Kjær online Library: http://www.bksv.com/Library.aspx

Croatian encyclopedia, online edition. Lexicographic Institute Miroslav Krleža, 2020. Accessed July 31, 2020 <http://www.enciklopedija.hr/Natuknica.aspx?ID=61734>.

Dan Russel: Acoustics and Vibration Animations: http://www.acs.psu.edu/drussell/demos.html

harmoničko titranje. Hrvatska enciklopedija, mrežno izdanje. Leksikografski zavod Miroslav Krleža, 2020. Pristupljeno 31. 7. 2020. <http://www.enciklopedija.hr/Natuknica.aspx?ID=24438>.

Institute of Sound and Vibration – Sound Waves: http://resource.isvr.soton.ac.uk/spcg/tutorial/tutorial/StartCD.htm

jakost. Hrvatska enciklopedija, mrežno izdanje. Leksikografski zavod Miroslav Krleža, 2020. Pristupljeno 31, 15(30), 5-13.

Moving acoustics (Visualisation Module): http://www.ta.chalmers.se/education.php?page=moving

The New Criteri Hrvatska enciklopedija, internetsko izdanje. Leksikografski zavod Miroslav Krleža, 2020. Pristupljeno 31. srpnja 2020. <http://www.enciklopedija.hr/Natuknica.aspx?ID=63768>.

William M. Hartmann: Principles of Musical Acoustics, Springer, 2013

Geometry for a Symmetric 2-Path Atom Interferometer Model

Yakubu Adamu
University of Aberdeen, UK, yakubua29@gmail.com

Clarles H-T. Wang
University of Aberdeen, UK

Abstract: It is often argued that the sensitivity of atom interferometer depends on the geometry of the interfering atom paths, conventionally, atom interferometer are usually configured to be sensitive to all deformations including tensor and scalar field deformations, it is a promising and robust tool for obtaining a highly sensitive and accurate measurements of gravitational signals, as such they are potentially capable of testing a wide range of fundamental physics questions including gravitational decoherence. Therefore, motivated by the recent search to improve the sensitivity of the next generation atom interferometer, we derived an expression, which defines the geometry of the interfering paths for a 2-level atom interferometer model, and in doing so, we further analysed various configurations for the geometric interpretation, in addition to interferometric influence phase shift and a possible decoherence factor which could lead to a systematic theoretical framework for future sensing of weak forces, due to, for example, gravitational waves and light dark matter.

Keywords: Geometry, interferometer, phase shift, two-level atom, symmetry

Introduction

The science of atom interferometry has developed very rapidly in past few decades, making them a unique choice for future quantum sensing of weak forces, due to, for example gravitational wave and light dark matter. They are potentially capable of detecting gravitational waves and scalar fields as well as ensuring little interaction with unwanted environmental influences, such as electric and magnetic fields (Bongs et al, 2019). However, the present-day sensisity of the next generation atom interferometer would require a significant improvement in order to test for many fundamental physics questions including gravitational decoherence. To this end, improving the sensitivity of atom interferometer and setting higher limits for the search for ultra- light dark matter can offer an unprecedented potential for new discoveries. Therefore, in this paper, we derived a broad class of geometric equations for a symmetric 2-path atom interferometer model which obeys specific time configuration that would help in improving the sensitivity of the next generation atom interferometer.

Here, we consider equation (5.20) of Wang and Adamu (2019), which represents the interference effect of the 2-path atom interferometer with translational degrees of freedom.

$$\tilde{d}(\boldsymbol{k},t) = \hbar\Omega_o e^{-i\omega t}\int_0^t dt'\, e^{-i(\boldsymbol{k}.r_1(t')-\omega t')} - \hbar(A\Omega_o - a\omega_o)e^{-i\omega t}\int_0^t dt'\, e^{-i(\boldsymbol{k}.r_2(t')-\omega t')} \quad (1.1)$$

where $r_1(t')$ and $r_2(t')$ are the classical path of the atom with respect to time, $\hbar\omega_o$ is a kinetic term that described the transition frequency of the atom and $\hbar\Omega_o$ is the total mass-energy transition of the atom and *a* and *A* are some coupling coefficients.

Two-Path Atom Interferometer Model

For our model, we consider a quantum particle in 2-level atom model, which experience a linearly varying potential otherwise free and described by the Hamiltonian density

$$\mathcal{H}_{SI} = \mathcal{H}_0 + \delta(\boldsymbol{x}-\boldsymbol{r}(t))\,\hbar\big[\omega_0(1+a\,\phi)|e\rangle\langle e| - A\,\Omega_0\phi\big] \quad (1.2)$$

Adamu, Y. & Wang, C. H-T. (2020). Geometry for a Symmetric 2-Path Atom Interferometer Model. In V. M. Bradley & I. Sahin (Eds.), *Proceedings of iLSET 2020-- International Conference on Life Sciences, Engineering and Technology* (pp. 26-29), Washington, DC, USA. ISTES Organization.

This follows the parameters described by Eq.(1.1) where $\mathcal{H}_{SI}$ is system interaction Hamiltonian density, $\mathcal{H}_o$ is a kinetic term. For the sake of simplicity, we assumed that a quantum particle which is initially $(t' = 0)$ split into the spatially separated classical two paths $r_1(t')$ and $r_2(t')$ after been kicked by a photon momentum and recombines at $(t' = t)$. The initial quantum states associated with the two paths are given respectively by $|\Psi_1(0)\rangle$and $|\Psi_2(0)\rangle$ so that the total initial state takes the form.

$$\Psi(0) = \frac{1}{\sqrt{2}}\left(|\Psi_1(0)\rangle + |\Psi_2(0)\rangle\right) \tag{1.3}$$

corresponding to the density matrix

$$\rho(0) = \frac{1}{\sqrt{2}}\left(|\Psi_1(0)\rangle\langle\Psi_1(0)| + |\Psi_2(0)\rangle\langle\Psi_2(0)| + |\Psi_1(0)\rangle\langle\Psi_2(0)| + |\Psi_2(0)\rangle\langle\Psi_1(0)|\right) \tag{1.4}$$

By using (1.2), we can then define the states withs respect to the atom paths as follows:

$$|\Psi_1(0)\rangle = |g\rangle\ |r_1(t')\rangle \tag{1.5}$$

$$|\Psi_2(0)\rangle = |g\rangle\ |r_2(t')\rangle \tag{1.6}$$

The perspective for this model is that when laser light interact with atomic particle in the interferometer, the atoms are coherently driven from the ground to an excited states in an oscillatory manner. Taking into account the photon momentum, caused by laser pulses which create a superposition of momentum states, the excited part of the superposition will then move away from the ground state, and thus travel simultaneously along different paths as described in Figure 1. Although paths may differ in height, but for this model we assumed that they are symmetric such that the 2 part in Eq (1.1) will meet continuously, in a way that the resulting interference phase will depend on the gravitational potential difference between the trajectories (Neder et al., 2006), and by so doing the interferometer becomes a very sensitive gravity sensor.

Geometry for Interferometer Model

To describe the interferometer geometry for the model, let us consider Figure 1, which shows a 2-path r_1 and r_2 configuration (color-lines), this form an interferometer to be described by equation (1.1). Here, we assumed that the two arms, r_1 and r_2, of the interferometer will experience accelerations $r_1(t')$ and $r_1(t')$ respectively at time t, which we shall define from $t' = 0$ at the initial state of the interferometer as shown in Fig. 1.

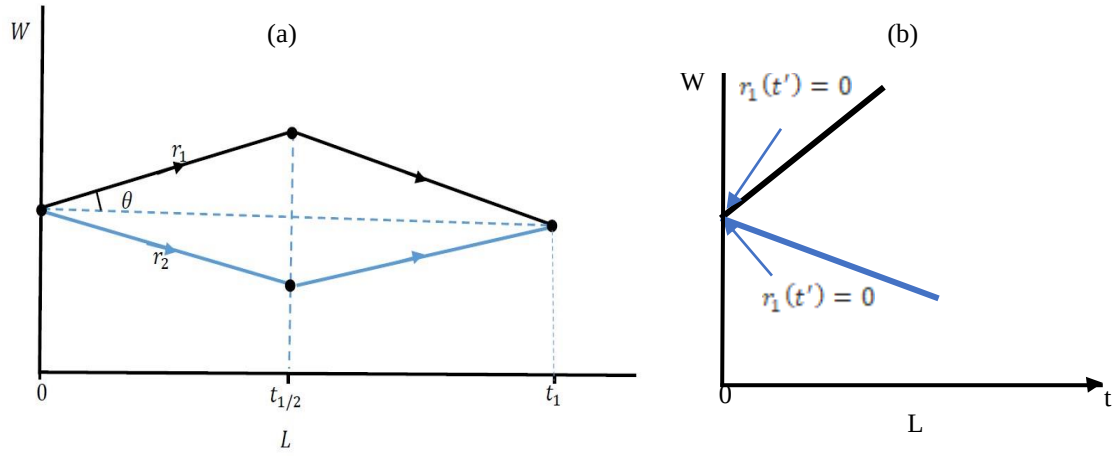

Figure 1. (a) Symmetric 2-path atom interferometry in the absence of gravity. (b) The acceleration kick on the quantum particle along the paths due to photon momentum. The 2-paths r_1 and r_2 satisfies the symmetry properties described in Eq. 1.1. such that the two-paths recombines at (t') continuously.

The starting point of this approach is based on the classical action of atom-light interaction. We assume that the atom is in a inertial frame of reference at $t' = 0$ (see Figure 1b), and the action of laser light-atomic interactions would affect the motion of the atom, which would leads to linear displacements of the atom into

different trajectories of the symmetric 2-paths. The classical action allows us to calculate the interferometer geometry and the exact interferometer phase shift for the moder under consideration.

Therefore, to calculate the interferometer geometry, the following expressions describe the symmetric 2-path configuration for the classical paths r_1 and r_2 with length L and width W. In this expression we consider only the integral of the potential term, such that the two paths are governed by coordinate components of the specified paths. Hence

$$r_1(t) = \begin{cases} (cos\theta\ vt,\ sin\theta\ vt, 0), & if\ 0 < t < t_{1/2} \\ \left(\frac{L}{2} + cos\theta\ vt,\ \frac{W}{2} - sin\theta\ vt,\ 0\right), & if\ t_{1/2} < t < t_1 \end{cases} \quad (1.7)$$

$$r_2(t) = \begin{cases} (cos\theta\ vt,\ -sin\theta\ vt, 0), & if\ 0 < t < t_{1/2} \\ \left(\frac{L}{2} + cos\theta\ vt, -\frac{W}{2} + sin\theta\ vt,\ 0\right), & if\ t_{1/2} < t < t_1 \end{cases} \quad (1.8)$$

where $cos\theta\ vt$, $sin\theta\ vt$ etc are the coordinate component along $r_1(t)$ and $r_2(t)$ paths respectively and $\tan\theta = W/L$ and $vt = \sqrt{W^2 + L^2}$. Now, evaluating equation (1.1) using the explicit components of $r_1(t)$ and $r_2(t)$ for the total time sequence labeled by (t), we have the following

$$\begin{aligned} \partial(\boldsymbol{k}, t_1) = \hbar\Omega_o e^{-i\omega t_1} \int_0^{t_1/2} dt'\, e^{-i(\boldsymbol{k}, r_1(t) - \omega t)} \\ -\hbar(A\Omega_o - a\omega_o) e^{-i\omega t_1} \int_0^{t_1/2} dt'\, e^{-i(\boldsymbol{k}, r_2(t') - \omega t')} \\ + \hbar\Omega_o e^{-i\omega t_1} \int_{t_1/2}^{t_1} dt'\, e^{-i(\boldsymbol{k}, r_1(t) - \omega t)} \\ -\hbar(A\Omega_o - a\omega_o) e^{-i\omega t_1} \int_{t_1/2}^{t_1} dt'\, e^{-i(\boldsymbol{k}, r_2(t') - \omega t')} \end{aligned} \quad (1.9)$$

Then by substituting the various components into eq.(1.9) and using exponential rule, it follows that

$$\partial(\boldsymbol{k}, t) = i\hbar A\Omega_0 e^{-i\omega t_1} \frac{(e^{-i\Omega_+ t_1/2} - 1)}{\Omega_+} - i\hbar A\Omega_1 e^{-i\omega t_1} \frac{(e^{-i\Omega_- t_1/2} - 1)}{\Omega_-}$$

$$+ i\hbar A\Omega_0 e^{-i(k_x L/2 + k_x L/2)} e^{-i\omega t_1} \frac{(e^{-i\Omega_+ t_1} - e^{-i\Omega_+ t_1/2})}{\Omega_+} - i\hbar A\Omega_1 e^{-i(k_x L/2 + k_x L/2)} e^{-i\omega t_1} \frac{(e^{-i\Omega_- t_1} - e^{-i\Omega_- t_1/2})}{\Omega_-} \quad (1.10)$$

The value of $\partial(\boldsymbol{k}, t)$ using (1.10) represents the interference effect due the geometric configuration for the 2-path interferometer. The diamond geometry described in figure 1. can be used to maximize the sensitivity of the interferometer phase to potential gradients.. This configuration (diamond geometry) is suitable to measure time-controllable gradients in a differential scheme.

Phase functional for 2-path Model

The phase functional for the atom interferometer model presented here is calculated based on the classical action of atom-light interaction. We assumed that the system is coupled to a stationary reservoir and in a Gaussian state, so that the dissipation and the noise kernel are respectively

$$\mathcal{D}(x - x') := \frac{1}{\hbar}\langle\{\emptyset(x), \emptyset(x')\}\rangle_R \quad \text{and} \quad \mathcal{N}(x - x') := \frac{1}{\hbar}\langle\{\emptyset(x), \emptyset(x')\}\rangle_R \quad (1.11)$$

can be introduced by using Eq.1.4 being the reduced density matrix of the matter at the initial time $(x' = 0)$. Thus, by introducing both the dissipation and noise kernel

$$\rho(x) = T_{\leftarrow}^{Q}\left(\exp\left[\int_0^4 d^4x^4 \mathcal{L}_s^{self}(x') + \frac{1}{2\hbar}\int_0^4 d^4x' \int_0^4 d^4x'' \{i\mathcal{D}(x'-x'')(Q_+(x') - Q_-(x'))(Q_+(x') - Q_-(x')) + \mathcal{N}(x'-x'')(Q_+(x') - Q_-(x'))(Q_+(x') - Q_-(x'))\}\right]\right)_{\rho(0)} \quad (1.12)$$

This leads to the influence phase functional

$$i\Phi[q_1, q_2] = -\frac{1}{2\hbar}\int_0^t d^4x' \int_0^{t'} d^4x'' \{i\mathcal{D}(x'-x'')(q_1(x') - q_2(x'))\,(q_1(x'') + q_2(x'')) + \mathcal{N}(x'-x'')(q_1(x') - q_2(x'))\,(q_1(x'') - q_2(x''))\} \quad (1.13)$$

(1.21)

is the effective influence phase functional for the 2-path model and the associated decoherence functional is given by the real part of $i\Phi[q_1, q_2]$.

Conclusion

In summary, we have derived a broad class of equations represent a geometric factors for a symmetric2-path atom interferometer model. We proved that the model presented here have the capability to measure time-controllable gradients thereby achieving a solution which can improve the sensitivity of atom interferometer. The equations established here would allow us to better engineered an effective interferometer paths which would laid both the theoretical and experimental foundation that are needed in understanding the concepts and theories of applications for sensing weak forces for example, gravitational wave.

References

Bongs, K., Holynski, M., Vovrosh, J., Bouyer,P., Condon, G., Rasel, E., Schubet, C., Schleich, W.P., and Roura, A. (2019)*Taking atom interferometric quantum sensors from the laboratory to real-world applications. Nat Rev Phys* **1,** 731–739. https://doi.org/10.1038/s42254-019-0117-4

Neder, I., Heiblum, M., Levinson, Y., Mahalu,D. and Umansky, V. (2006) *Unexpected Behavior in a Two-Path Electron Interferometer*, Phys. Rev. Lett., vol. 96, no. 1, p. 016804

Wang, C. H.-T. and Adamu, Y. (2019). *Decoherence in an atom interferometer due to light dark matter*. ResearchGate, Reprint of Unpublish Manuscript.

Impact of Small Organic Molecules on the Stability and Conformational Flexibility of Globular Proteins

Tatyana Tretyakova
LEPL I. Beritashvili Center of Experimental Biomedicine, Georgia, tatitre@gmail.com

Maya Makharadze
LEPL I. Beritashvili Center of Experimental Biomedicine, Georgia

Sophio Uchaneishvili
LEPL I. Beritashvili Center of Experimental Biomedicine, Georgia

Dimitri Khoshtariya
LEPL I. Beritashvili Center of Experimental Biomedicine, Georgia
Ivane Javakhishvili Tbilisi State University, Georgia

Abstract: Profound understanding of mechanisms governing proteins' function is one of the major goals of both fundamental and applied biomedical sciences. Recent theoretical and experimental studies showed that protein function is essentially linked to its structure, stability and conformational flexibility, which in turn can be drastically altered by the crowded intracellular environment of proteins. The aim of presented research is to investigate an impact of nonspecific organic additives, urea and dimethyl sulfoxide (DMSO), on the conformational properties of model globular protein, hen egg albumin (HEA). We applied differential scanning microcalorimetry to measure thermodynamic parameters of HEA thermal unfolding in presence of wide range of additives concentrations. Our resent experiment revealed that HEA exhibited gradual destabilization in whole range of buffered urea solutions (0-30% urea in PSB, pH8.0), manifested through monotonic decrease of melting temperature and significant decrease of enthalpy which is not concentration dependent within the experimental range of concentrations. However, in presence of the same concentrations of DMSO (PSB, pH8.0), we observed slight increase of the melting temperature and enthalpy in 5% DMSO solution, followed by gradual decrease of both thermodynamic parameters with increase of DMSO concentration. Experimental results obtained for interaction of HEA with DMSO are qualitatively similar to our previous findings on α-chymotrypsin and could be explained by change of preferential solvation of water against DMSO, which was never observed in denaturizing urea solutions. Low concentrations of DMSO remotely strengthen bond water networks of the protein protecting it from unfolding, whereas subsequent increase of DMSO concentration leads to gradual destabilization of the protein. This work was supported by Shota Rustaveli National Science Foundation of Georgia (SRNSFG) grant YS-18-2034 and is a part of systematic fundamental research on the intrinsic links between protein stability, conformational flexibility and function.

Keywords: Protein stability, differential scanning calorimetry, urea, dimethyl sulfoxide

Introduction

Profound understanding of mechanisms governing proteins' function is one of the major goals of both fundamental and applied biomedical sciences. Recent theoretical and experimental studies showed that protein function is essentially linked to its structure, stability and conformational flexibility, which in turn can be drastically altered by the crowded intracellular environment of proteins. The aim of presented research is to investigate an impact of nonspecific organic additives, urea and dimethyl sulfoxide (DMSO), on the conformational properties of model globular protein, albumin from chicken egg white (EA). DMSO is a small organic molecule widely used in research and medicine, which is able to cause both, stabilization or destabilization of globular proteins, while urea is known as a denaturant. EA is one of the serpin superfamily proteins having a well-studied structure, but not much is known about its function. Presumably it has only a storage function.

Tretyakova, T., Makharadze, M., Uchaneishvili S., & Khoshtariya, D. (2020). Impact of Small Organic Molecules on the Stability and Conformational Flexibility of Globular Proteins. In V. M. Bradley & I. Sahin (Eds.), *Proceedings of iLSET 2020-- International Conference on Life Sciences, Engineering and Technology* (pp. 30-32), Washington, DC, USA. ISTES Organization.

Method

We applied differential scanning microcalorimetry (DSC) to measure thermodynamic parameters of EA thermal unfolding in presence of wide range of additives concentrations. Calorimetric measurements were carried out using a DASM-4 adiabatic scanning calorimeter (Biopribor, Russia). The heating rate was 2 K/min throughout all experiments.

DSC is a very powerful experimental method for the investigation of a thermodynamic stability of globular proteins under the impact of various organic additives. It allows for a direct measurement of the biomolecule's enthalpy and plotting partial heat capacity as a function of temperature. From the recorded DSC curves the melting temperature T (melting peak x-coordinate), transition enthalpy ΔH (melting peak area) and other thermodynamic parameters can be calculated (Tretyakova et al, 2013).

Results

We carried out two experimental series in the alkaline media, namely 0.1 M phosphate buffer solution (pH8) containing no additive, 5, 10, 20 and 30 % of urea or DMSO (see Figure 1). Our experiments revealed that EA exhibited gradual destabilization in whole range of buffered urea solutions (0-30% urea in 0.1 M PBS, pH8), manifested through monotonic decrease of melting temperature and enthalpy. However, in presence of the same concentrations of DMSO (0.1 M PBS, pH8), we observed slight increase of the melting temperature and enthalpy in 5% DMSO solution, followed by gradual decrease of both thermodynamic parameters with increase of DMSO concentration (see Table 1 for details).

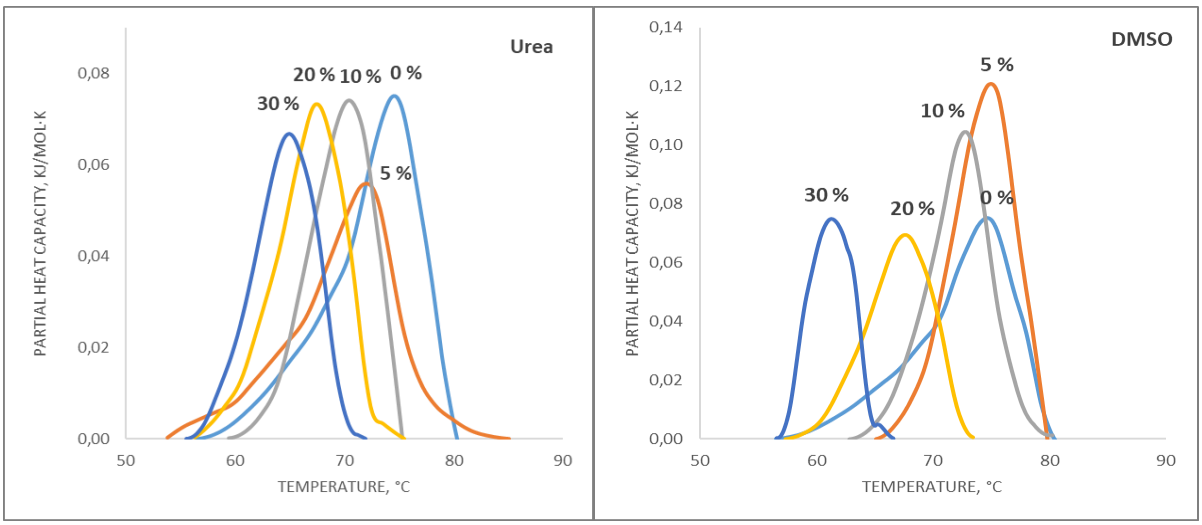

Figure 1. DSC Curves for the EA Thermal Unfolding in the Presence of 0–30% Urea and DMSO Concentrations

Table 1. Calorimetric Enthalpy and Melting Temperature for the Thermal Unfolding of the EA in the Presence of Different Additives Concentrations

Additive concentration, %	Urea		DMSO	
	ΔH_{cal} (kJ/Mol)	T_m, °C	ΔH_{cal} (kJ/Mol)	T_m, °C
0	243	74	243	74
5	204	72	285	75
10	191	70	239	73
20	173	68	174	67
30	169	65	131	62

Conclusion

Experimental results obtained for interaction of EA with DMSO are qualitatively similar to our previous findings on α-chymotrypsin (Tretyakova et al., 2013) and could be explained by change of preferential solvation of water against DMSO, which was never observed in denaturizing urea solutions (Auton Bolen, & Rösgen, 2008, Batista et al., 2013, Nnyigide, Lee, & Hyun, 2018). Low concentrations of DMSO remotely strengthen bond water networks of the protein protecting it from unfolding, whereas subsequent increase of DMSO concentration leads to gradual destabilization of the protein. Additional study on the impact of urea and DMSO on conformational properties of EA in acidic medium (pH6) is scheduled to gain more information on the solvation effects.

Acknowledgements

This work was supported by Shota Rustaveli National Science Foundation of Georgia (SRNSFG) grant YS-18-2034.

References

Auton, A., Bolen, D. W., & Rösgen, J. (2008) Structural thermodynamics of protein preferential solvation: Osmolyte solvation of proteins, aminoacids, and peptides. *Proteins: Structure, Function, and Bioinformatics, 73 (4), 802-813.*

Batista, A. N. L., Batista, Jr, J. M., Bolzani, V. S., Furlan, M., & Blanch, E. W. (2013). Selective DMSO-induced conformational changes in proteins from Raman optical activity. *Phys. Chem. Chem. Phys., 15, 20147-20152.*

Nnyigide, O. S., Lee, S. G., & Hyun, K. (2018). Exploring the differences and similarities between urea and thermally driven denaturation of bovine serum albumin: intermolecular forces and solvation preferences. *Journal of Molecular Modeling, 24-75.*

Tretyakova, T., Shushanyan, M., Partskhaladze, T., Makharadze, M., van Eldik, R., & Khoshariya, D. (2013) Simplicity within the complexity: Bilateral impact of DMSO on the functional and unfolding patterns of α-chymotrypsin. *Biophysical Chemistry, 175-176, 17-27.*

Digital Twins for Education and Study of Engineering Sciences

Serge Zacher
University of Applied Sciences Darmstadt, Faculty EIT, Germany, info@szacher.de

Abstract: Digital twins, used by education and engineering, are software-models of industrial plants, which are simulated and visualized similar to its industrial originals and synchronized with them. In the paper are shown steps of design of digital twins upon some examples of the master degree program at University of Applied Sciences Darmstadt. It will be described why and how it is possible to use the digital twins. The different stages of the development of software-models, which are equipped with different levels of source code will be shown. The advantages of digital twins for engineering study including the economic considerations will be discussed.

Keywords: Simulation, model-in-the-loop, software-in-the loop, processor-in-the-loop, digital twin

Introduction: The Way to Digital Twins

The practical exercises on the real technological devices are supposed as a necessary part by the study of engineering sciences at universities. To reduce high costs for building their own well-equipped laboratories the universities use hardware-models of industrial processes, which are usually boxes with microcontrollers, located inside. The success of programming has opened a new way of costs reducing, namely: the software-models (Figure 1). But as low are costs for software-models, they cannot replace the real industrial devices.

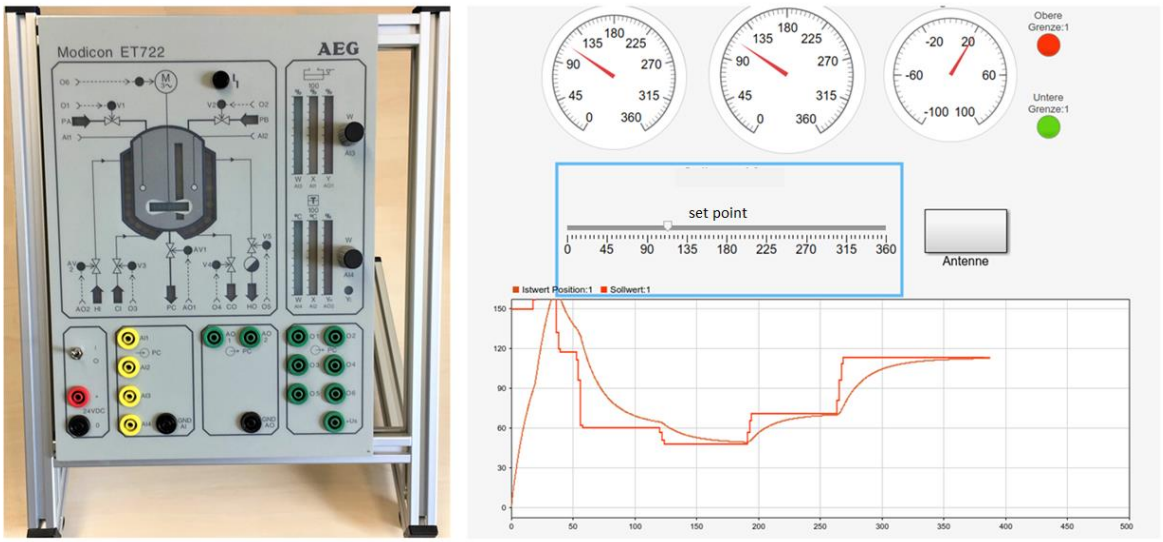

Figure 1. Hardware-model of a Batch-rector as a Laboratory Device (on the left) and its Software-model

Another way to do practical exercises on the real devices is remote control or so called Web Lab (Henry, 1998; Henry & Zacher, 2010a, 2010b). The global digitalization of information, known as “Industry 4.0” concept, has led in the industry and also by laboratories of engineering study to so called “digital twins” (Piascik et al., 2010). A digital twin is simulated and visualized software-model, which is synchronized with the original system and operates in the real time (Figure 2).

Zacher, S. (2020). Digital Twins for Education and Study of Engineering Sciences. In V. M. Bradley & I. Sahin (Eds.), *Proceedings of iLSET 2020-- International Conference on Life Sciences, Engineering and Technology* (pp. 33-36), Washington, DC, USA. ISTES Organization.

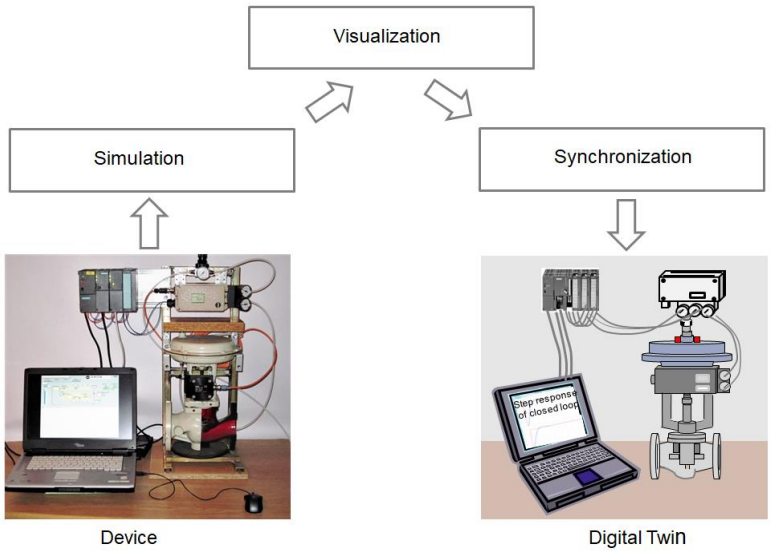

Figure 2. Developments Stages of Digital Twins for Study and Education

From MIL to PIL and HIL

The following options of digital twins are possible (Figure 3):

- Model-in-the-loop (MIL), if software-models of a plant and of a controller interact on only one host PC.
- Software-in-the-loop (SIL), if the controller code is executed together with the software-model of the plant on the same host.
- Processor-in-the-loop (PIL), if software-model of a plant is executed on one host (usually on a PC) and the controller code is implemented on another host (usually on a microcontroller board).

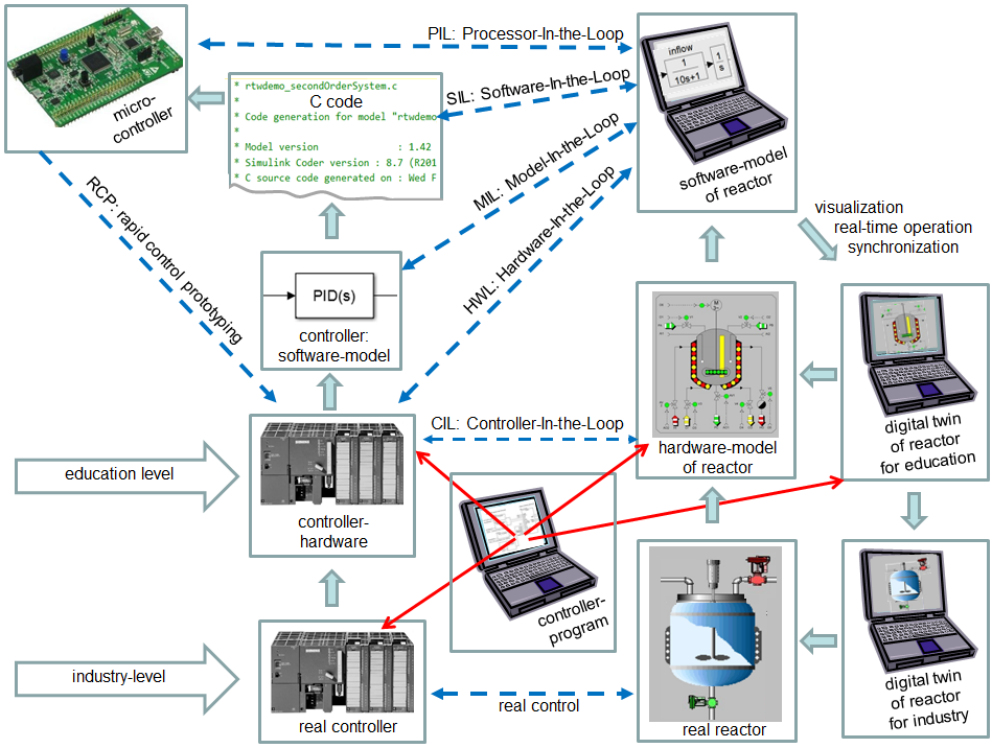

Figure 3. Classification of Hardware- and Software-models

Experiences about Digital Twins by Engineering Study

An example of digital twin and videos can be found in (Szabo, & Gurkasch, 2018) In Figure 4, the digital twin developed in (Lutz & Herbst, 2019) and used in (Czwalina, Gilung, Jeckel, & Heymann, 2019) for practical exercises by university courses such as “Automation” or “PLC” is shown.

The following problems by using the digital twin were found:

- The real-time capability can be lost, if the simulation system does not offer the necessary performance.
- The visualization and animation depends on software platform (MS Windows or MacOS).
- The 90 comparators were necessary to display the level of real device with MATLAB® with LEDs.

Figure 4. Digital Twin (l.) Simulated and Controlled by [6] with MATLAB ®/Simulink. The Hardware-model OSLO-3 (r.) Controlled with PLC Freelance and Field Controller AC-700 of ABB.

In Figure 5, a digital twin of a mechatronic device, which was designed by project team (Freitag, Alonso Gonsalez, & Buhl, 2020) for learning purposes to be transportable and therefore suitable for demonstration in the classroom, is shown. As a control device was chosen an S7-1215C CPU of SIEMENS. The conveyor was simulated very close to reality, depending on the speeds of the conveyor belt. However, it was observed that considerable resources are required even for this relatively simple simulation task.

Figure 5. Conveyor model (l.) designed by [8] with the CAD SIEMENS NX and its digital twin animated with MCD software (Mechatronics Concept Designer from SIEMENS)

Conclusions

The numerous advantages make digital twins an indispensable tool in today's university world. The benefits of digital twins are:

- Easy preparation for the training or experiments.
- No hardware is required to be installed or tested.
- An unlimited number of people can work with digital twins and apply them.
- The internship with digital twins can be made as comfortable as in classic laboratory rooms.

The disadvantage by creating a digital twin is the design effort, which is only one-off. Also the high costs for CAD-licences belong to a disadvantage. However the whole costs savings by the use of digital twins in an education laboratory consisting of fifteen laboratory places are 26% against fifteen real devices.

References

Czwalina, D., Gilung, W., Jeckel, T., & Heymann, J. (2019). *PLCopen für digitalen Zwilling des OSLO-3.* Hochschule Darmstadt, FB EIT, Fernmaster Studiengang, 2019. (accessed on the 29.01.2020): https://www.zacher-international.com/C22_Team_Projekt/PLCOpenOSLO/PLCOpenDigiZwi.pdf

Freitag, E., Alonso Gonsalez, C., & Buhl, J. (2020). *Digitaler Zwilling einer Förderanlage*, Hochschule Darmstadt, FB EIT, Fernmaster Studiengang, 2020. Video (accessed on the 29.01.2020): https://www.zacher-international.com/C22_Team_Projekt/DigiZwi/DigZwi_Foerderstrecke.mp4

Henry, J. (1998). *Laboratory teaching via the WWW*. – In: ASEE Southeast U.S. Annual Meeting, 1998

Henry, J., & Zacher, S. (2010a). *Description of the remote UTC-WebLab for engineering education and interactive demonstration with online experiments*. International Conference "Remote Engineering & Virtual Instrumentation" REV, KTH, Stockholm, Sweden, June 29-July 02, 2010

Henry, J., & Zacher, S. (2010b): *WebLabs in Control Engineering Education: status and trends*. – In: 7. AALE Angewandte Automatisierung in der Lehre und Forschung, FH Technikum Wien, 10./11. Feb. 2010

Lutz, M., & Herbst, D. (2019). *Digitaler Zwilling der OSLO-Tafel*, Hochschule Darmstadt, FB EIT, Fernmaster Studiengang, 2019. Video (accessed on the 29.01.2020): https://www.zacher-international.com/C22_Team_Projekt/Digitaler_Zwiling_L_H/DZLH.mp4

Piascik, R., et al. (2010). *Technology Area 12: Materials, Structures, Mechanical Systems, and Manufacturing Road Map*. 2010, NASA Office of Chief Technologist.

Szabo, A., & Gurkasch, T. (2018). *Digitaler Zwilling der Simulationstafel ET722*, Seminararbeit DHBW Stuttgart, FB Technik, 2018. Video (accessed on the 20.01.2020): https://www.zacher-international.com/Projekte/DHBW_Stuttgart/ET722_DigZwi/ET722_DigZwi_Sz_Gur.mp4